Optical and Structural Effects of Copper Doping on 2D Layered $(BA)_2PbCl_4$ Perovskite

SAUMYA SEBASTIAN
(MS16083)

A dissertation submitted for the partial fulfilment of

BS-MS dual degree in Science

Indian Institute of Science Education and Research Mohali

April 2021

Certificate of Examination

This is to certify that the dissertation titled "**Optical and Structural Effects of Copper Doping on 2D Layered $(BA)_2PbCl_4$ Perovskite**" submitted by **Ms. Saumya Sebastian (Reg. No. MS16083)** for the partial fulfilment of BS-MS dual degree programme of the Institute, has been examined by the thesis committee duly appointed by the Institute. The committee finds the work done by the candidate satisfactory and recommends that the report be accepted.

Dr. Angshuman Roy Choudhury
(Local/Administrative Guide)

Dr. Santanu Kumar Pal

Dr. Subhabrata Maiti

Dr. Debrina Jana
(Supervisor)

Dated: April 30, 2021

Declaration

The work presented in this dissertation has been carried out by me under the guidance of Dr. Debrina Jana at the Indian Institute of Science Education and Research Mohali. This work has not been submitted in part or in full for a degree, a diploma, or a fellowship to any other university or institute. Whenever contributions of others are involved, every effort is made to indicate this clearly, with due acknowledgement of collaborative research and discussions. This thesis is a bonafide record of original work done by me and all sources listed within have been detailed in the bibliography.

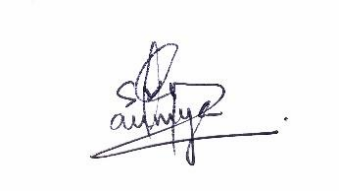

Saumya Sebastian
(Candidate)

Dated: April 30, 2021

In my capacity as the supervisor of the candidate's project work, I certify that the above statements by the candidate are true to the best of my knowledge.

Dr. Debrina Jana
(Supervisor)

Acknowledgements

I would like to express my sincere gratitude and graceful acknowledgment to my supervisor Dr. Debrina Jana for her guidance and valuable support towards the completion of this work.

I gratefully acknowledge INSPIRE faculty grant of Dr. Debrina Jana and Notional allocation fund of IISER Mohali for funding this work. I am thankful to IISER Mohali central research facility for doing the XRD and SEM and Department of Science and Technology, India for providing INSPIRE scholarship throughout my academic program.

I would like to express thanks to my Local/Administrative guide Dr. Angshuman Roy Choudhury, project committee members Dr. Santanu Kumar Pal and Dr. Subhabarta Maiti for their time and valuable suggestions that improved me to think more scientifically and understand the basic phenomena.

I am thankful to the Department of Chemical Science, IISER Mohali for providing departmental teaching laboratory and other experimental facilities. I also thank the computer center for their computational facilities, the library for grating us access to a wide spectrum of information, the office of dean academics for maintaining my academic records and making my study process smooth, the office of dean students for hostel, mess facilities, and office of registrar and accounts for my fellowship and other financial and other administrative matters.

I would like to acknowledge IIT Roorkee for XPS and IISER BHOPAL for EPR.

I express my gratitude to Mr. Deepraj Verma who worked along with me in the completion of this thesis work.

I am grateful to my lab members Ms. Neha Bajaj and Mr. Akhilesh Meena for being supportive lab members. I express my gratitude to Ms. Labhini Singla, Mr. Mayank Joshi and Dr. Mrinal K. Adak for accommodating us in their lab and providing us the necessary infrastructure. I would also like to thank my seniors Ms. Ashitha P.P for her help and guidance.

Finally, yet importantly, I express my sincere gratitude to my beloved parents for their blessings, my siblings for their constant support and my friends for their help and wishes for the successful proceedings of this project work.

Saumya Sebastian

List of Figures

Notations and Abbreviation

SEM	Scanning electron Microscopy
PXRD	Powder X-ray Diffraction
EPR	Electron paramagnetic resonance
FTIR	Fourier transform infrared
DRS	Diffuse Reflectance Spectroscopy
XPS	X-ray Photoelectron Spectroscopy
TGA	Thermo-Gravimetric Analysis
RP	Ruddlesden Popper
DJ	Dion Jacobson
ACI	Aurivillius
SCXRD	Single Crystal X-ray Diffraction
LED	Light Emitting Diode
UV	Ultraviolet
EDS	Energy Dispersive X-ray Spectroscopy.

CONTENTS

Abstract

Two dimensional perovskites have emerged as interesting candidates for optoelectronic and photovoltaic applications due to their enhanced stability and tunability options. Doping perovskites enable altering their optoelectronic properties to achieve exciting properties. In this thesis, two dimensional perovskites $(BA)_2PbCl_4$ was synthesised and doped with Copper. Their optical, structural and electronic properties were characterised using DRS, PXRD, SEM, EPR, XPS, FTIR and thermal properties were analysed using TGA. Doping was found to reduce the bandgap of $(BA)_2PbCl_4$ from 3.5 eV to 2.3 eV. The doped compound exhibited good thermal and moisture stability and has an optimal bandgap which makes them good candidates for photovoltaic applications.

Chapter 1

INTRODUCTION

1.1 PEROVSKITES

Materials with a structure similar to the first discovered perovskite mineral $CaTiO_3$ are termed perovskites.[1] Metal halide Perovskites have the general formula ABX_3 and adopt the perovskite structure where A is the large cation occupying the cuboctahedral position. B is the small transition metal, usually divalent with a coordination number of 6 occupying the centre of the corner-sharing octahedra formed from the halide X ions.[2]

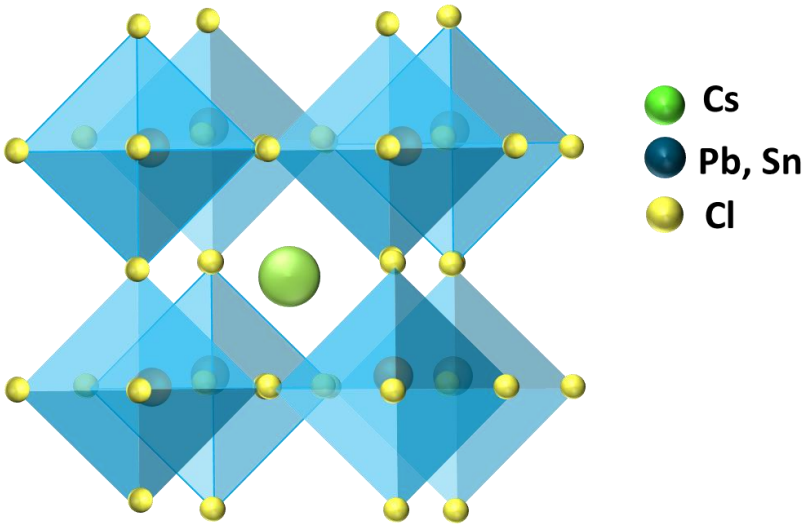

Figure 1. Perovskite structure.

The stability of the perovskite structure is dictated by the Goldschmidt tolerance factor given by

$$T = \frac{(r_A + r_x)}{\sqrt{2}(r_B + r_x)}$$

Where r_A, r_x, r_x are the ionic radii of the ions. The ideal perovskite has a cubic structure, with t=1 but perovskites with orthorhombic, rhombohedral and tetragonal crystal structure

having lower t values ranging between 0.75 and 1 are more common.[3] This distortion of the structure arises from the small A site cations which causes a tilting of the octahedra to optimize A-X bonding. The Goldschmidt tolerance constraint restricts the possible combination of elements that can form stable 3D perovskites.

Perovskites have high optical absorption coefficients and exhibit narrow-band bright photoluminescence, in addition to their halide-dependent tunable bandgaps, low exciton binding energies, and long-range carrier diffusion[4]. They exhibit fewer trap states despite containing a large number of defects, making them defect tolerant. These materials find extensive application in optoelectronics and photovoltaics owing to their easy synthesis and processability, near-unity Photoluminescence Quantum Yield (PLQY) and wide absorption range.[5]

1.2 TWO DIMENSIONAL PEROVSKITES

Two-dimensional perovskites are formed when large A-site cations are incorporated into the space between the octahedra. This leads to the breakdown of the structure to 2D where insulating A site cations act as spacers between the layers of inorganic BX_6- octahedra.

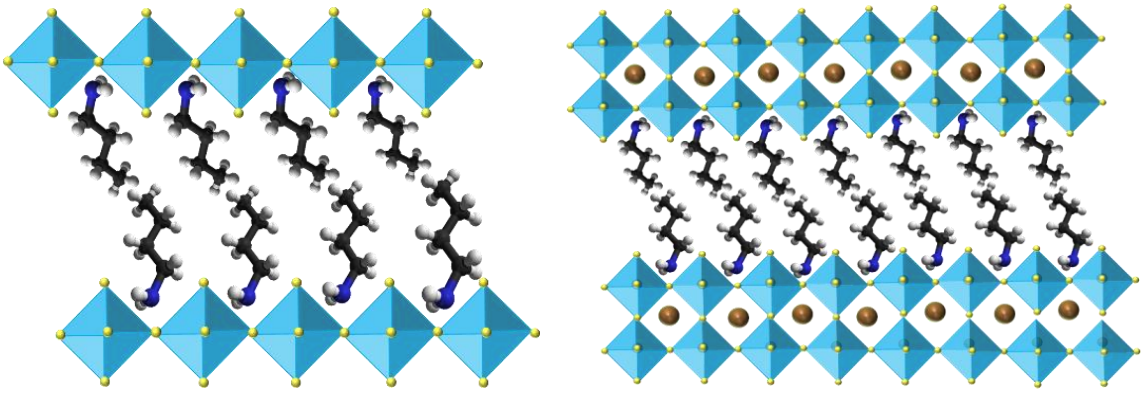

n = 1 n = 2

Figure 2. Two dimensional Ruddlesden Popper (RP) perovskites with varying number of inorganic layers n=1 and n=2.

This dimensional reduction gives access to a large plethora of hybrid organic-inorganic materials with tailorable functionalities and structural complexities which allows for the fine-tuning of optoelectronic properties.[6] Some of the A site cations include butylammonium, ethyl ammonium, benzylammonium, iodobenzylammonium etc.

These 2D structures offer large compositional flexibility allowing control of the structural distortion, quantum and dielectric confinement, exciton-phonon coupling and Rashba splitting, which in turn modulate their optical, electronic and spin properties.[6] The alternating layers of conducting inorganic layers and insulating organic layers generate a quantum well-like structure.[7] The presence of the large organic spacer cations in between the inorganic halide octahedrons also enhances their moisture stability, which was a major concern for 3D perovskite.[8] These properties have attracted 2D perovskites for use in optoelectronic and photovoltaic applications.

1.3 STRUCTURAL MODES

Corner sharing between octahedra is the most common connectivity mode among 2D perovskites which is further classified into <100>, <110> and <111> oriented structures based on the crystallographic orientation of the stacking of the inorganic layers. <100> and <110> oriented forms have the general formula of $A'_2A_{n-1}B_nX_{3n+1}$ or $A'A_{n-1}B_nX_{3n+1}$, A′- the large spacer cation, A, the cation filling the octahedral void, B the metal ion and X is the halide, where n stands for the number of inorganic layers, while <111> has a general formula of $A'_{n+1}B_nX_{3n+3}$. The <100> oriented structures are further divided into Ruddlesden Popper (RP), Dion Jacobson (DJ) and Aurivillius (ACI) phases. The A-site cations of RP phases have a charge of +1 and cause the inorganic layers to be staggered by half a unit cell. To maintain charge neutrality of the crystals, two layers of organic spacer layer occupy in between the inorganic layers. The DJ phase consists of a single layer of +2 charged spacer cations between vertically stacked inorganic layers.[9] In the ACI phase, the A-site cation is present inside the octahedral cages as well as in the spacer layer alternating between another spacer cation.[10] Ruddlesden popper perovskite has been the most explored perovskites amongst the three, made using a large variety of spacer cations and synthesis methods.

1.4 SYNTHETIC ROUTE FOR 2D PEROVSKITES

1.4.1 Synthesis using hydrohalic acid.

A saturated solution of the metal source and spacer cation is dissolved in hydrohalic acid by heating and then cooled to room temperature once a clear solution is obtained. The number of inorganic layers can be controlled by changing the stoichiometry of the spacer cation added.[11]

1.4.2 Colloidal synthesis using organic solvents.

A saturated solution of the spacer, metal and halide source is made in organic solvent which upon cooling or heating depending on the solubility dependence of the precursors in the solvent, give rise to mixed-phase perovskite crystals.[12] Further optimisation of solvents, reaction conditions and stoichiometric control of the precursors need to be done to obtain phase pure perovskites.

1.4.3 Vapour Diffusion

The stoichiometric ratio of precursors dissolved in a good solvent is kept in a small vial which is placed inside a larger vial containing a bad solvent (antisolvent). The vapours of the antisolvent diffuse into the good solvent, causing the perovskite crystals to precipitate out. [12]

1.4.4 Solvothermal synthesis

Precursors dissolved in an appropriate solvent is sealed inside an autoclave or pyrex and subjected to high pressure, temperature and other reaction conditions to obtain 3D and 2D phases of perovskites.[13]

1.4.5 Solid-state grinding method

A stoichiometric amount of the precursors is ground together using a mortar and pestle to obtain the desired perovskite which is further annealed to obtain better quality crystals.[14] The crystals made using this method is not suitable for SCXRD.[12]

1.5 PROPERTIES OF 2D PEROVSKITES

1.5.1 Electronic structure

The valence band of 2D perovskite is predominantly composed of halide p orbitals and s orbitals of metals, while its conduction band is composed of p orbitals.[15] The presence of organic layers with low dielectric constant alternating with inorganic layer of high dielectric constant leads to dielectric confinement, resulting in strongly bound excitons with enhanced exciton binding energies.[16] The large binding energy promotes radiative recombination which makes them interesting candidates for high efficiency LEDs.[17] The band structure and alignment varies according to the metal, halide and the dielectric contrast between the organic and inorganic layers.

1.5.2 Effect of organic layer

Organic cations change the bandgap energy and lead to different biexciton binding energies depending on the dielectric contrast between organic and inorganic layer. The length of the alkyl chain of the organic layer also influences the bandgap of the perovskite.[18]

1.5.3 Effect of inorganic layer

The bandgap of 2D perovskite is influenced by both the metal cation and the halide used. Substituting lead with Sn leads to lowering of the bandgap and improves conductivity.[19] Using a more electronegative halide in place of Iodine leads to lowering of the valence band, resulting in increased bandgap.[20]The bandgap decreases with increasing layer number.[21]

1.5.4 Charge transport

Out of plane charge conductivity is limited due to the presence of high resistivity organic layer. As the number of inorganic layers between alternating organic layer increases, significant increase in the conductivity along the plane perpendicular to the sheets is observed.[18] Decreasing the length of the organic spacer can significantly enhance the out - of -plane charge transport.[22] Spacer ligands with aromatic moieties enhance out of plane charge conductivity and photovoltaic performance.[23]

1.6 DOPING in 2D PEROVSKITES

Relatively few works on the effect of doping of 2D perovskites have been done. Cesium doping on the n=3 analogue of the $(BA)_2(MA)_{n-1}Pb_nI_{3n+1}$ family helped synthesise crystals with controlled crystal orientation, increased grain size, and lower surface defects. The solar cell manufactured using the doped analogue gave a high power conversion efficiency of 13.7% with superior resistance to humidity.[24] Anupam.*et.al* effectively doped Mn^{2+} in $(BA)_2PbBr_4$ to obtain intense orange red emission due to enhanced energy transfer from the excitons of the host material to the d-electrons of Mn^{2+} ions.[25] Similar work on $(BA)_2PbBr_4$ single crystalline layered microcrystals was also performed by Dutta *et al*. Doping of Mn^{2+} on the other halide analogues of this system failed to produce significant changes in the emission characteristics.[26] $(BA)_2PbI_4$ has a bandgap of 2.4 eV[12] while $(BA)_2PbCl_4$ has a high bandgap of 3.6 eV and is non-luminescent[27] which restricts its usage in optoelectronic applications.

1.7 CURRENT WORK

$(C_4H_9NH_3)_2PbCl_4$ or $[(BA)_2PbCl_4]$ has a bandgap of 3.5 eV which is very high to be of use in photovoltaic applications. The compound is at the same time non-luminescent which limits its usage in optoelectronic applications as well. As discussed in previous sections, doping has been emerged as a potential tool for increasing the functionality of a perovskite material. There have been literature reports of effect of Copper doping on double perovskites with bandgap similar to that of $(BA)_2PbCl_4$. When white $Cs_2AgInCl_6$ with a bandgap of 3.6 eV was doped with Copper, the bandgap reduced to 2.19 eV and the compound changed its colour to yellow.[28] Doping $Cs_2SbAgCl_6$ with Copper helped tune its bandgap from 2.6 eV to 1 eV.[29] The goal of our current work is to explore the opportunities to increase the functionality of a 2D halide perovskite compound by appropriate doping. Firstly, encouraged by the literature reports on the significantly enhanced stability of 2D halide perovskites, we attempted to prepare $(BA)_2PbCl_4$ following the reported protocol. Secondly, we attempted to dope different metal ions e.g. Mn^{2+} and Cu^{2+} in order to understand the optical and structural effects, if any, the doping exerts on the system.

.

1.8 INSTRUMENTATION

Diffuse Reflectance spectra (DRS) of the crystals were measured using Cary 5000 UV-Vis-NIR spectrophotometer (Agilent technologies) from 280-800 nm range at a scan rate of 1 nm/s, using $BASO_4$ as the standard. Powder X-ray Diffraction (PXRD) data was recorded on Rigaku Ultima IV diffractometer enabled with Cu Kα (1.54 Å) radiation with a scan rate of 1º 2θ/min ranging from 5-60º. Field Emission Scanning Electron Microscopy (FESEM) was done using JEOL-7600F. Thermal Gravimetric Analysis (TGA) was performed using DTG-60H from Shimadzu with a heating rate of 5 ℃/min upto 800 ℃. X-ray photoelectron spectroscopy (XPS) was done using PHI 5000 VersaProbe III Model. Electron paramagnetic resonance (EPR) was done with a Bruker MicroX spectrometer in X band frequency (Microwave frequency 9.44 GHz) at room temperature. Fourier Transform Infrared (FTIR) characteristics were examined using Perkin Elmer from 400-4000 cm^{-1}.

Chapter 2

2.1 EXPERIMENTAL SECTION

2.1.1 Materials

Lead Chloride ($PbCl_2$, 99%, Alfa Aesar), Copper (II) Chloride dihydrate ($CuCl_2.2H_2O$, 99%, Sigma Aldrich), Copper Chloride (CuCl, 99%, Sigma Aldrich), Butylamine ($C_4H_9NH_3$, 99%, Sigma Aldrich), 1-Octadecene (ODE, 90 %, Sigma Aldrich), Hydrochloric acid (HCl, 37%, Emparta, Sigma Aldrich).

2.1.2 Synthesis of Butylammonium Chloride (BACl) salt

1ml butylamine was added dropwise to 3 ml of hydrochloric acid kept in an ice bath. The reaction was allowed to proceed for 2 hours, following which the reaction mixture was heated at 100℃ for 24 hrs to obtain white BACl salt. The obtained salt was washed with either acetone or ethanol, filtered using suction and stored in vacuum.

2.1.3 Synthesis of pure $(BA)_2PbCl_4$

$(BA)_2PbCl_4$ was prepared using a high temperature colloidal synthetic method. 0.1 mmol $PbCl_2$, 5 mmol BACl was added to a 50 ml round bottom flask with 0.3 ml HCl and 5 ml octadecene, heated to 120 ^{0}C for 15 min under high N_2 flow. The reaction mixture was then cooled to room temperature during which time white coloured crystals started precipitating down. 6ml ethyl acetate was further added to 5 ml of the reaction mixture and centrifuged at 2000 rpm for 2 min. The resulting white semi-crystalline flakes were then washed again with hexane by centrifuging at 2000 rpm for 2 min. The obtained crystals were filtered using hexane and stored for further characterisation.

2.1.4 Synthesis of Cu doped $(BA)_2PbCl_4$

0.1 mmol of $CuCl_2.2H_2O$ or CuCl was added along with reactants above and same reaction steps were followed to obtain yellow coloured doped $(BA)_2Cu_xPb_{1-x}Cl_4$.

2.2 RESULTS AND DISCUSSION

2.2.1 OPTICAL AND STRUCTURAL FEATURES OF $(BA)_2PbCl_4$

$(BA)_2PbCl_4$ contains single layer of inorganic Lead Chloride octahedron spaced using 2 layers of butylammonium ligand as shown in the schematic.

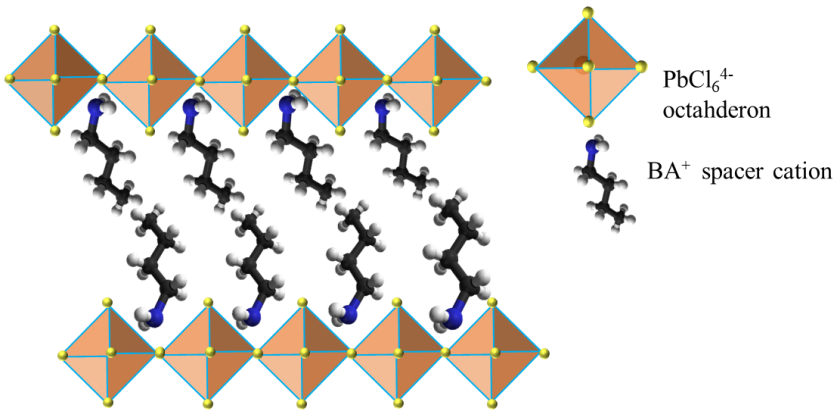

Figure 3. Schematic representation of $(BA)_2PbCl_4$ structure.

$(BA)_2PbCl_4$ was made using a high temperature solution based synthetic method. Lead Chloride was used as the metal source, BACl as the source of the spacer cation, octadecene as the solvent and HCl was used to dissolve the Lead precursor. The obtained crystals were white in colour and semicrystalline in nature.

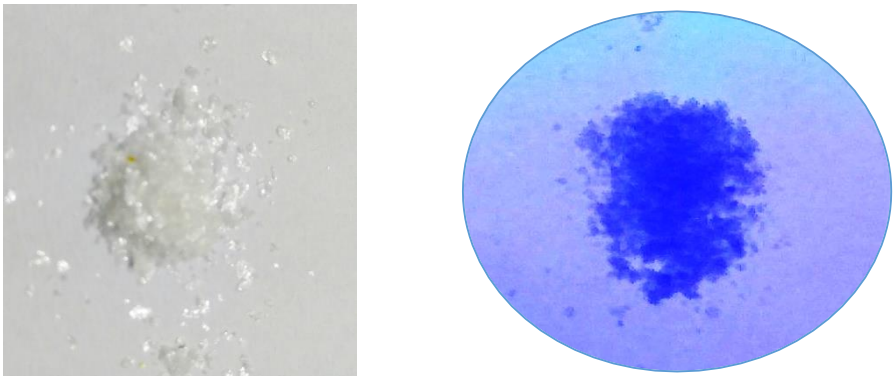

Figure 4. $(BA)_2PbCl_4$ under visible light and 365 nm UV light.

To understand the optical features of the system, diffuse reflectance spectra (DRS) was taken. The data obtained in absolute reflectance scale was converted to absorbance using Kubelka-Munk transformation[30]

$$\alpha \sim \frac{(1-R)^2}{2R}$$

R- absolute reflectance, α- pseudo absorbance.

From the absorbance data obtained, Tauc plot was created and bandgap calculated. The direct bandgap was measured by taking the intercept obtained by extrapolating the linear region of plot of $(\alpha hv)^2$ vs E(eV).

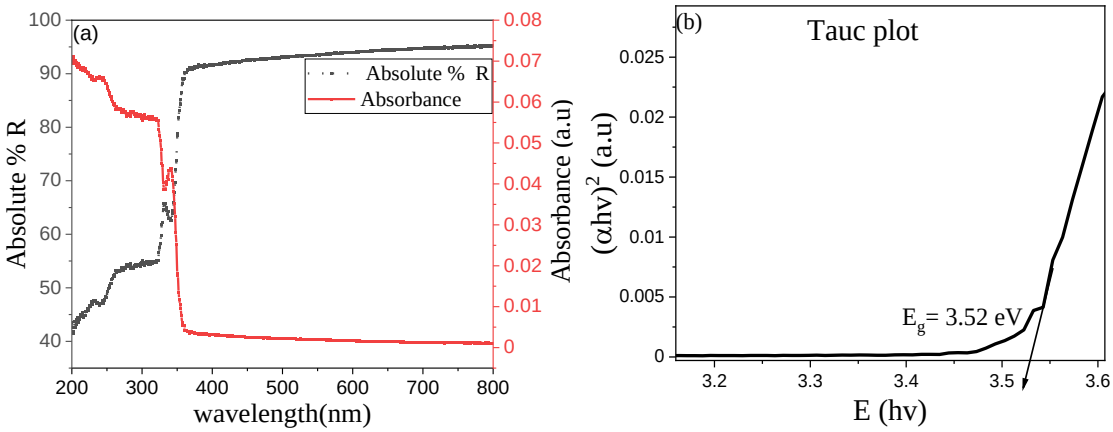

Figure 5. (a) DRS spectra of undoped $(BA)_2PbCl_4$. (b) Tauc plot of the corresponding absorbance spectra.

The undoped system had a sharp absorption peak at around 350 nm. Band gap of the undoped $(BA)_2PbCl_4$ was found to be 3.52 eV from the Tauc plot, which matches with literature values.[31] PXRD studies were done to understand the structure of pure sample.

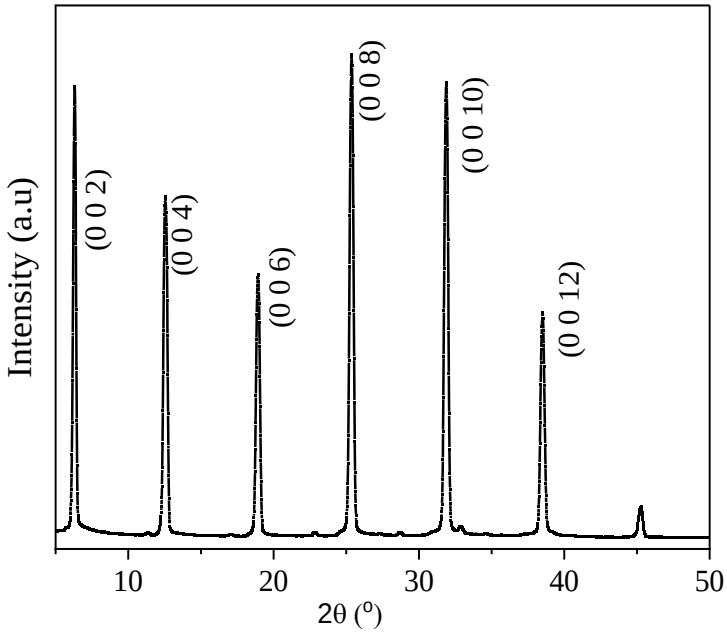

Figure 6. PXRD plot of $(BA)_2PbCl_4$.

The hkl values of $(BA)_2PbCl_4$ were taken from literature.[26] $(BA)_2PbCl_4$ has an orthorhombic crystal system with space group of $Cmc2_1$. The unit cell dimensions are a=7.98 Å, b=7.86 Å and c=27.79 Å .[30] The XRD peaks shows that the crystals formed are highly oriented along the c-axis with good crystallinity and purity.

2.2.2 OPTICAL AND STRUCTURAL PROPERTIES OF COPPER DOPED $(BA)_2PbCl_4$

Copper (I) Chloride and Copper (II) Chloride dihydrate (Chloride analogues of the dopant source) were selected to keep the halide component in the system same. Copper in both oxidation states were chosen to investigate whether changing oxidation state could influence the properties of the doped crystals. It is assumed that dopant Copper would replace Lead in the inorganic layers as shown in the figure.

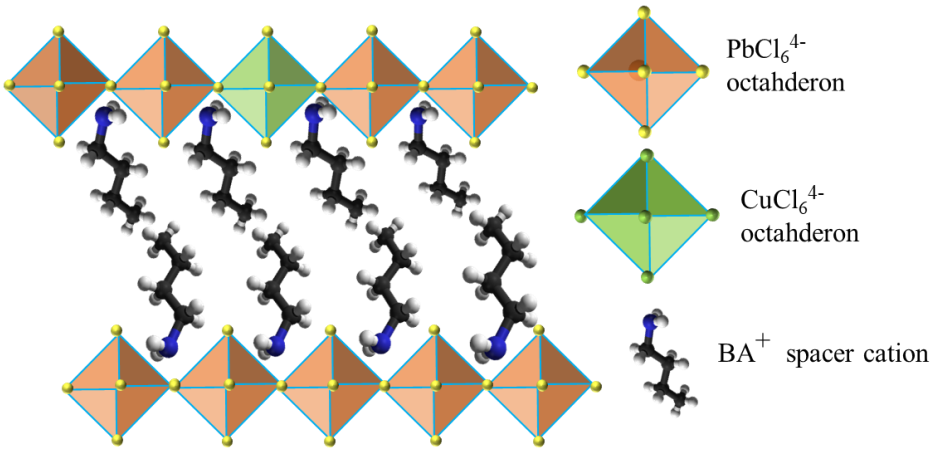

Figure 7. Schematic representation of Copper doping in $(BA)_2PbCl_4$.

The crystals turned yellow when doped with Cu. However, doping had no effect on the luminescent properties of the system. The doped crystals were non luminescent.

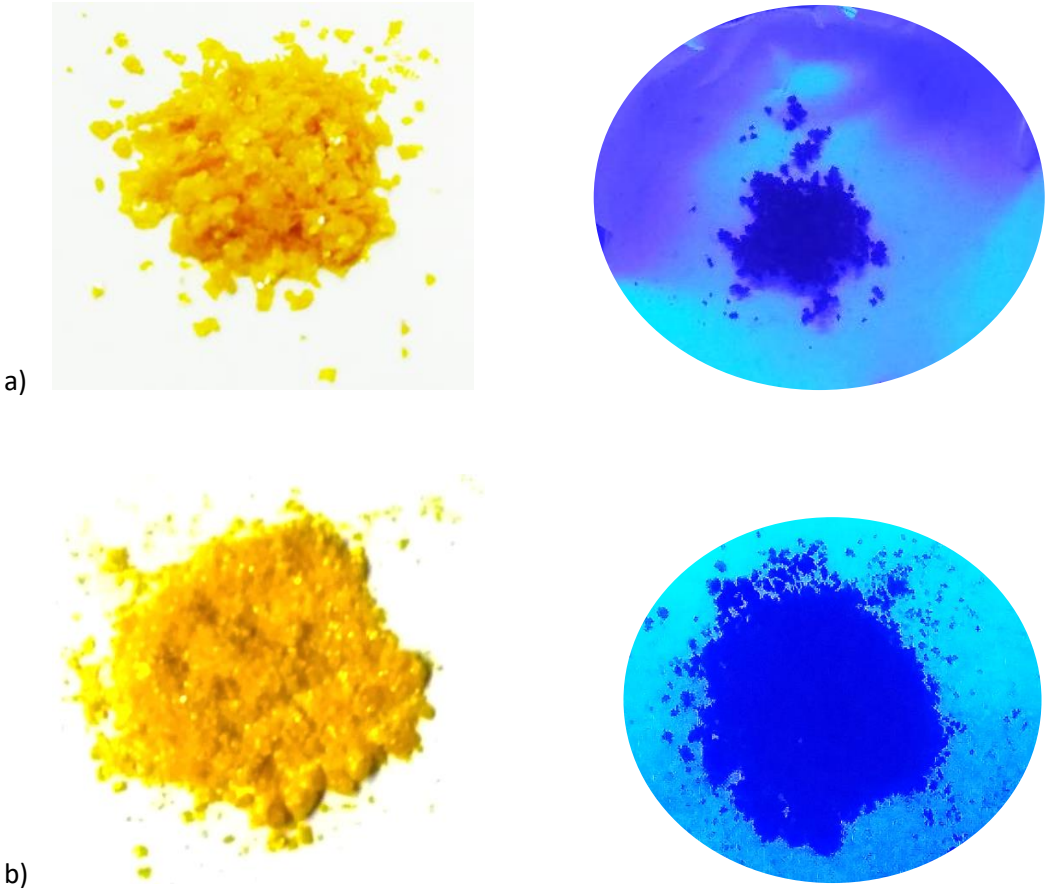

Figure 8. a) Cu^{2+} doped b) Cu^+ doped crystals under sunlight and UV light of 365 nm.

Upon doping the system with Copper (Cu^{2+}), the bandgap reduced to 2.3 eV observed from the Tauc plot; a broad absorption peak around 550 nm can be observed from the diffuse reflectance spectra (DRS) spectra.

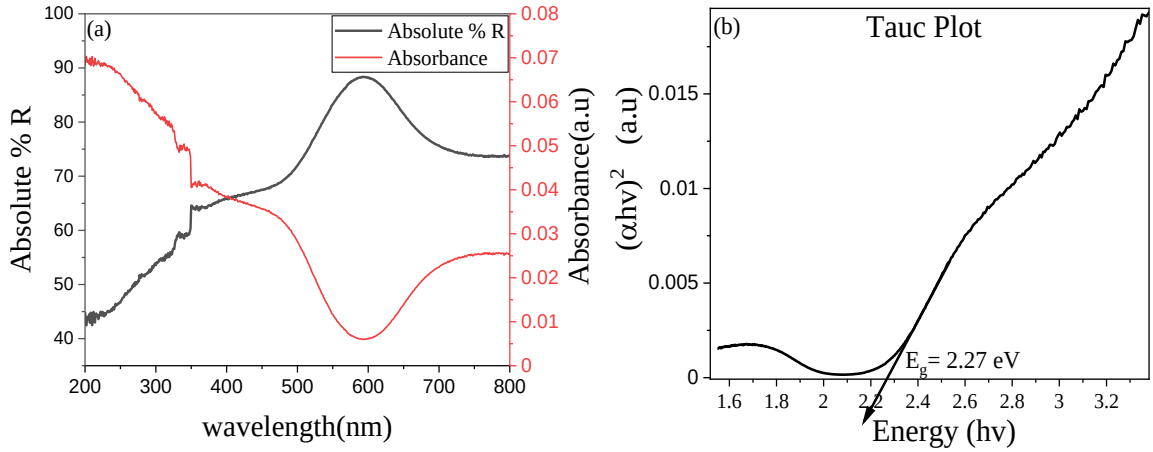

Figure 9. DRS spectra (a) and corresponding Tauc plot (b) of the $CuCl_2.2H_20$ (Cu^{2+}) doped $(BA)_2PbCl_4$.

Doping using CuCl also produced similar crystals with a lower bandgap of 2.3 eV and broad absorption peak at ~550 nm. From the optical spectral information, it can be inferred that both Cu^+ and Cu^{2+} dopants had similar effects on the optical properties of the system.

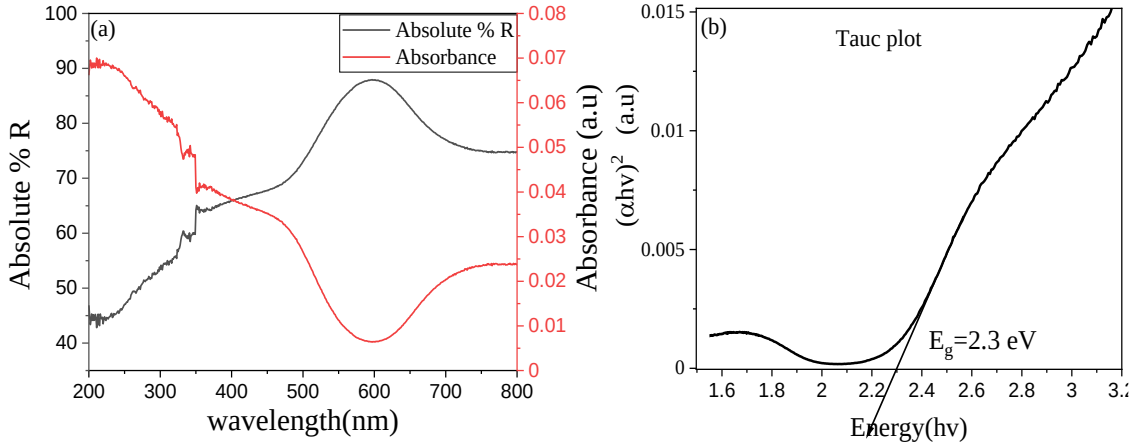

Figure 10. DRS spectra (a) and corresponding tauc plot (b) of Cu^+ doped $(BA)_2PbCl_4$.

To further study the structural effects of doping, PXRD of the doped samples were taken.

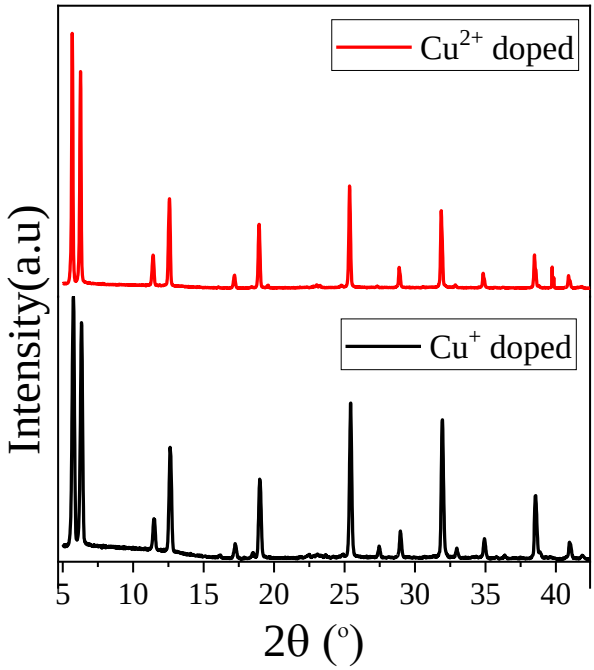

Figure 11. PXRD peaks of Cu^{2+} doped and Cu^{+} doped $(BA)_2PbCl_4$.

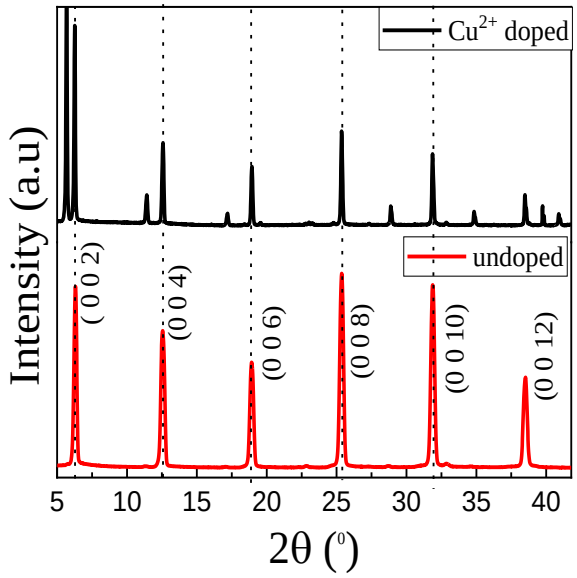

Figure 12. PXRD peaks of Cu^{2+} doped and undoped $(BA)_2PbCl_4$.

New peaks started appearing at lower angles with the introduction of Copper. The original peaks of the $(BA)_2PbCl_4$ diminished in intensity with Copper doping. Cu^{+} and Cu^{2+} doped systems have similar XRD peaks indicating that the structural effects induced by the dopants are the same.

2.2.3 CHARACTERISATION OF $(BA)_2PbCl_4$ AND COPPER DOPED $(BA)_2PbCl_4$

Electronic state of the elements (Pb, Cl, Cu) in the undoped and doped system were investigated using XPS.

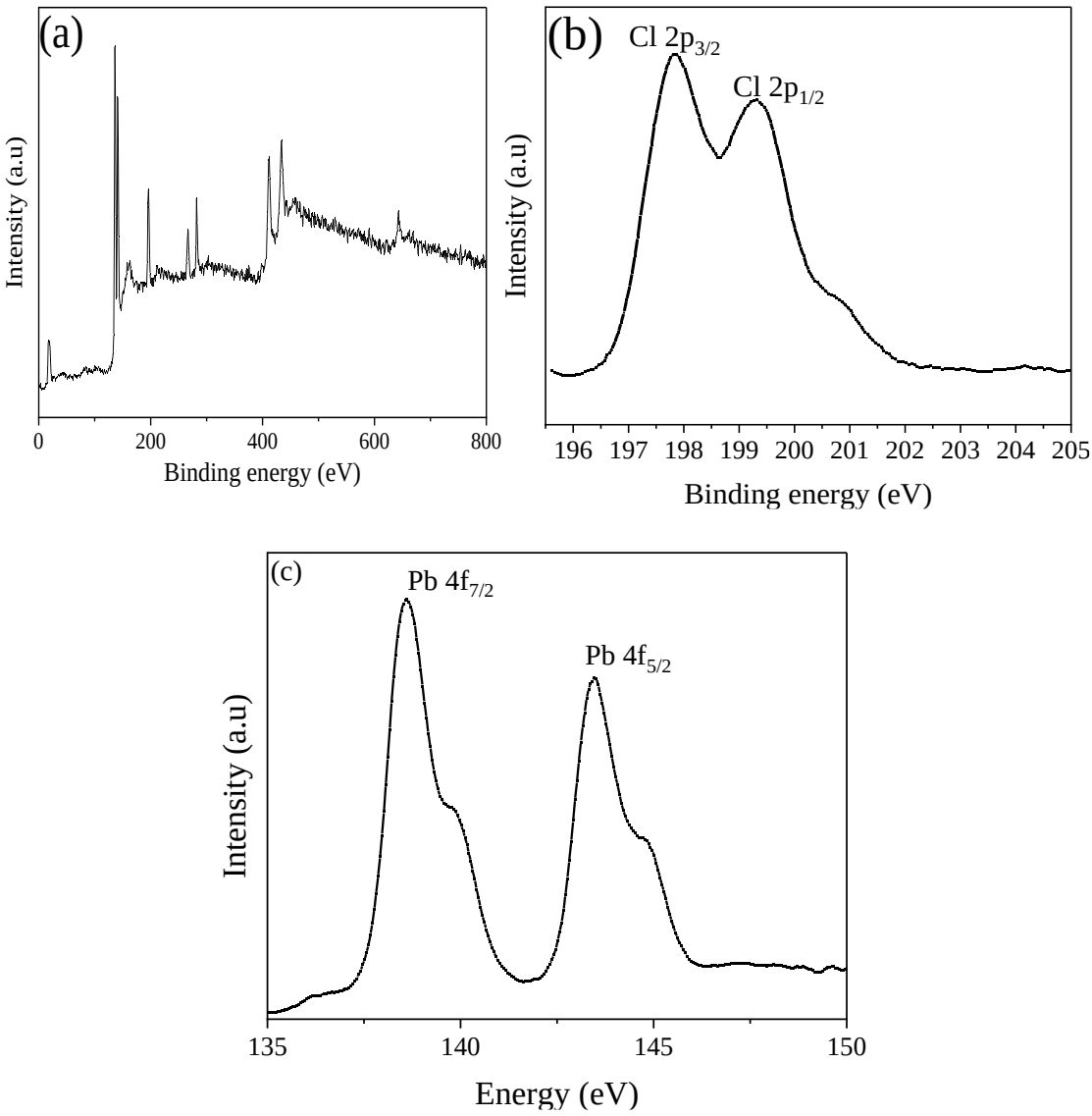

Figure 13. XPS data of $(BA)_2PbCl_4$ (a) survey scan (b-c) Cl, Pb.

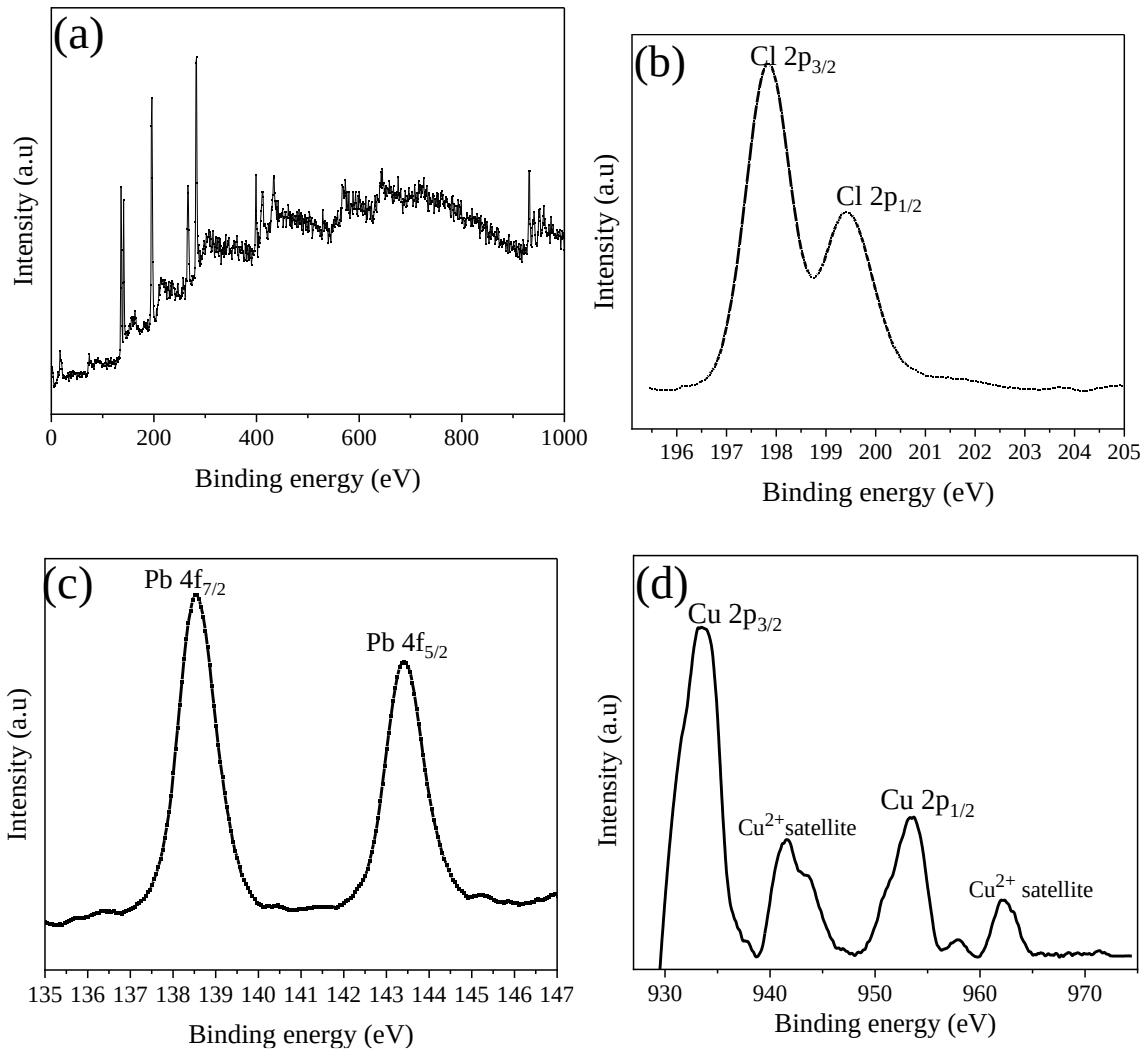

Figure 14. XPS Data of Cu^{2+} doped $(C_4H_9NH_3)_2PbCl_4$ (a) survey scan (b-d) Cl, Pb, Cu.

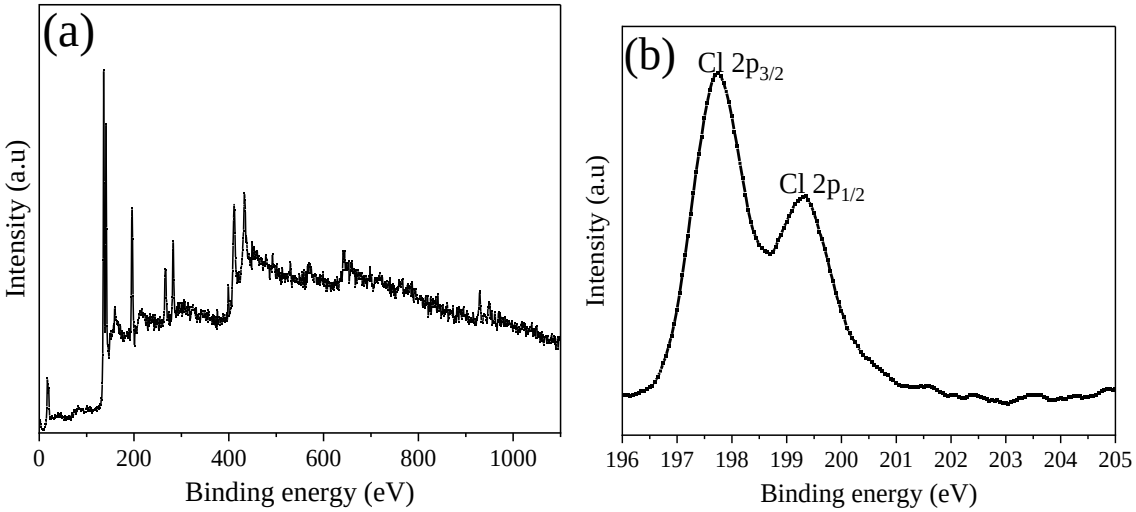

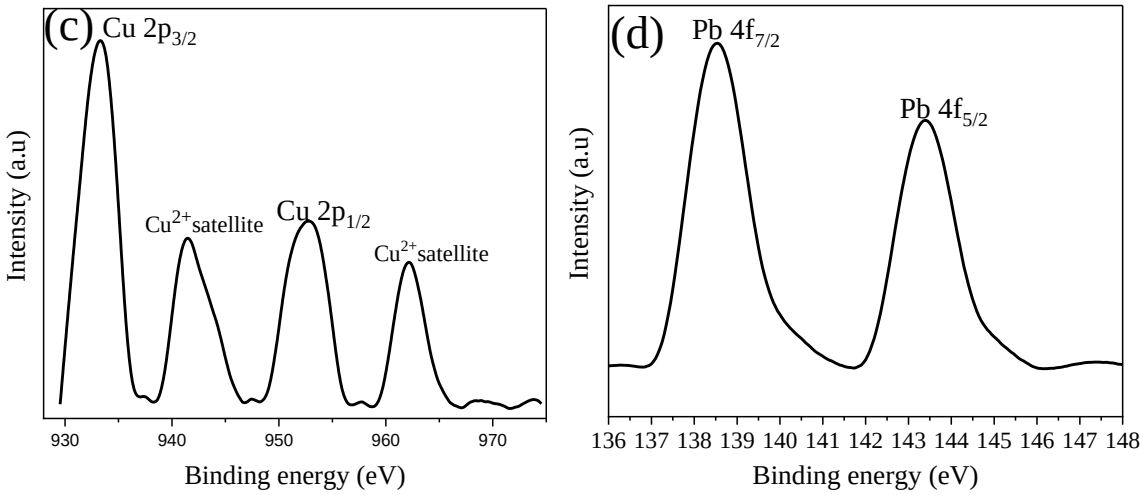

Figure 15. XPS Data of Cu^{+} doped $(C_4H_9NH_3)_2PbCl_4$ (a) survey scan (b-d) Cl, Cu, Pb.

The binding energy curves of Pb $4f_{7/2}$ and Pb $4f_{5/2}$ are observed at ~138.5 eV and 143.3 eV respectively, while the peaks of Cl $2p_{3/2}$ and Cl $2p_{1/2}$ are located around 197.7 eV and 199 eV. These results suggest that the constituent elements (Pb, Cl) are in their normal valence +2 and -1 respectively which mimics literature values.[32] The XPS data for the Copper element in both the Cu^{+} and Cu^{2+} sample shows the same kind of strong satellite peaks[33] that are indicative of the Cu^{2+} oxidation state. It can be concluded that Copper transforms into +2 oxidation state for the Cu^{+} doped $(BA)_2PbCl_4$.

To understand the electronic state and coordination environment of Copper in both Cu^{+} doped and Cu^{2+} doped $(BA)_2PbCl_4$, electron paramagnetic resonance data of both the samples were taken.

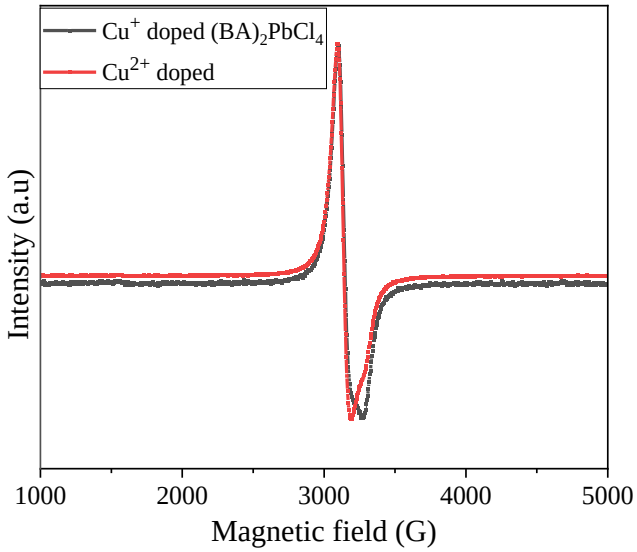

Figure 16. EPR data of Cu^{+} and Cu^{2+} doped $(BA)_2PbCl_4$.

The EPR signal shows a peak centred at 3130 Gauss which indicates Cu^{2+} presence in the system. Both Cu^{+} doped $(BA)_2PbCl_4$ and Cu^{2+} doped $(BA)_2PbCl_4$ has similar EPR peak position confirming the similarity of electronic and coordination environment. This is due to the presence of 1 unpaired electron in the d^9 configuration of Cu^{2+} with a total electron spin of S=1/2. Hyperfine splitting was not observed suggesting interaction between Cu (II) centres of the doped system.[34]

To further understand the influence of changing dopant concentration, 0.5 mmol, 1 mmol, 2 mmol, 3 mmol and 4 mmol of $CuCl_2.2H_2O$ was added along with 0.1 mmol $PbCl_2$ (Cu: Pb ratio- 0.5:1, 1:1, 2:1, 3:1, 4:1 respectively.). DRS and XRD of the synthesised compounds were taken and compared.

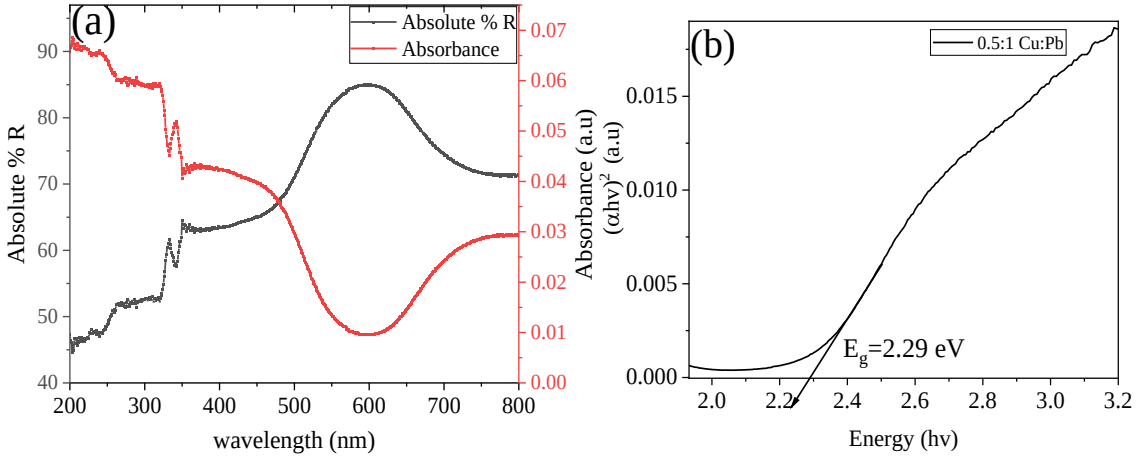

Figure 17. (a) DRS and (b) tauc plot of 0.5:1 [Cu:Pb] doped $(BA)_2PbCl_4$.

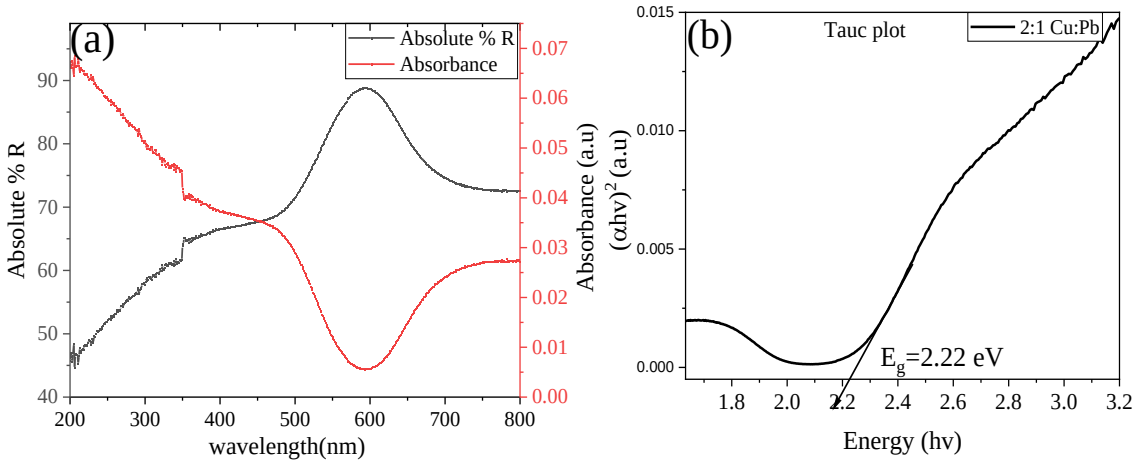

Figure 18. (a) DRS and (b) Tauc plot of 2:1 [Cu: Pb] doped $(BA)_2PbCl_4$.

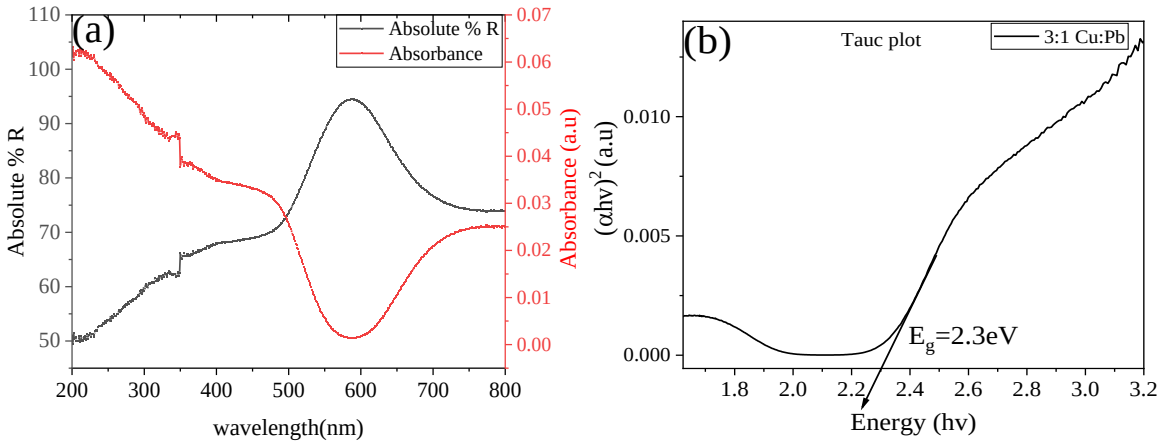

Figure 19. (a) DRS and (b) tauc plot of 3:1 [Cu:Pb] doped $(BA)_2PbCl_4$.

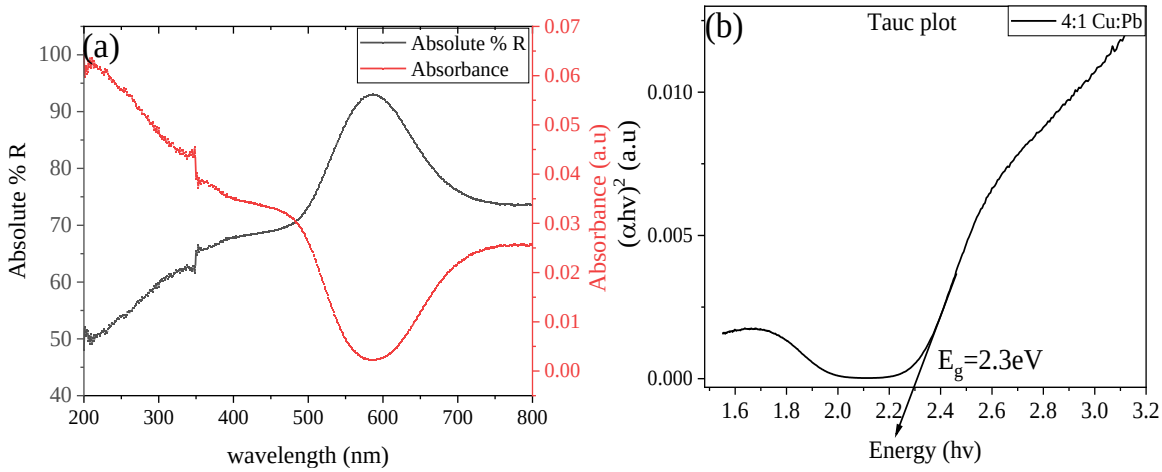

Figure 20. (a) DRS and (b) tauc plot of 4:1 [Cu:Pb] doped $(BA)_2PbCl_4$.

All the doped samples had a bandgap of ~2.3 eV regardless of the doping concentration. Increasing the dopant concentration to higher amounts had negligible effect on the absorption properties and bandgap of the system.

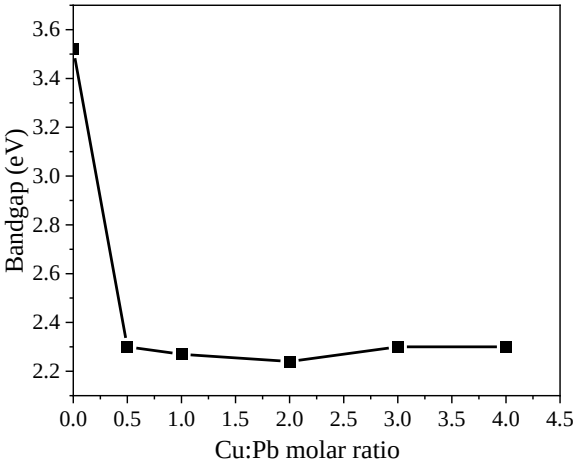

Figure 21. Variation of bandgap with increasing dopant concentration.

To further understand the structural changes induced by varying the dopant concentration, powder XRD of the doped samples were analysed.

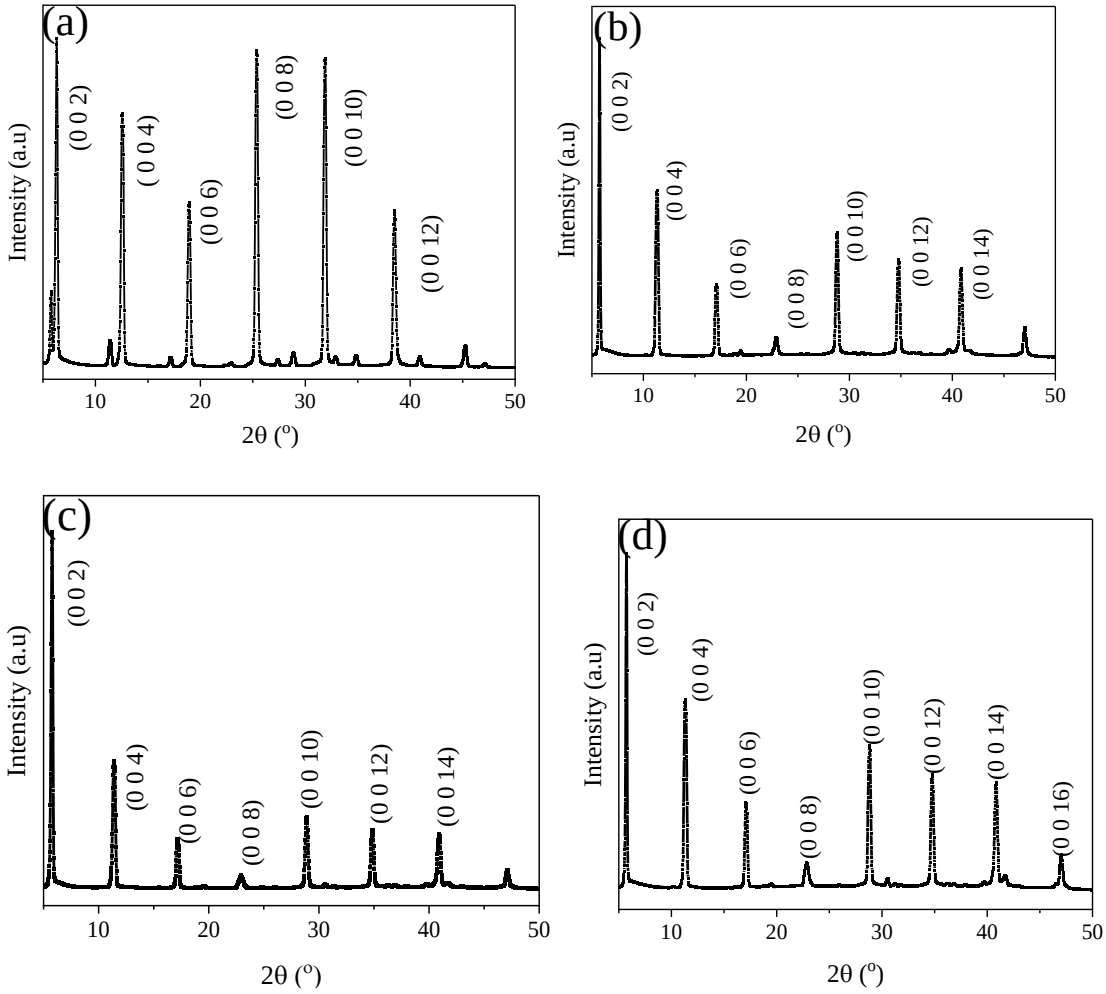

Figure 22. PXRD of the doped $(BA)_2PbCl_4$ with Cu:Pb ratio of (a) 0.5:1 (b) 2:1 (c) 3:1 (d) 4:1.

PXRD was done to compare the peak shifts occurring on varying the dopant concentration from low to high concentration.

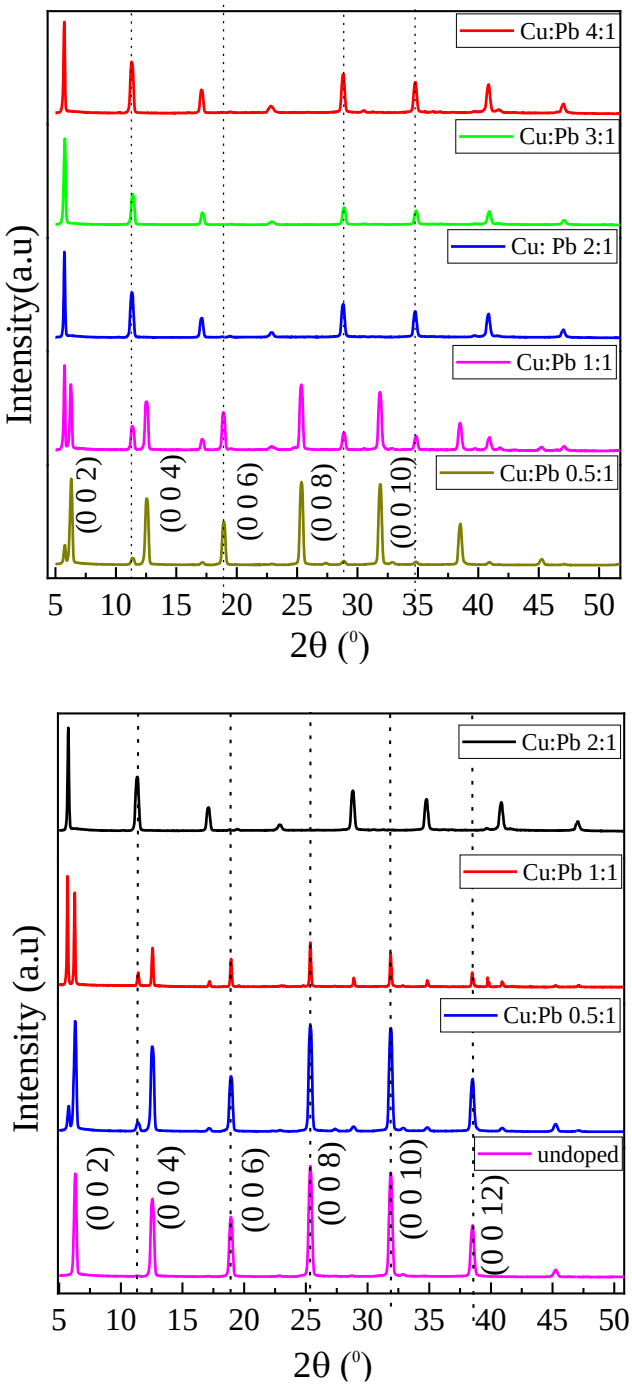

Figure 23. PXRD comparison of doped $(BA)_2PbCl_4$ crystals.

On increasing the dopant concentration, new peaks started appearing at lower angles. The original peaks of the undoped samples diminished in intensity on incrementing dopant concentration and completely disappeared when the amount of Cu in the reaction mixture was twice that of the Pb concentration. The d spacing of the undoped samples were

calculated to be 14.041 and the d spacing values for the 2:1 Cu:Pb doped samples was found to be 15.499. Similar d spacing values and PXRD pattern was observed for $(BA)_2CuCl_4$, in literature.[35] These results indicate that Copper completely replaces Lead in the system on increasing the dopant concentration. To further confirm this, SEM, EDS and elemental colour mapping of the undoped, 0.5:1, 1:1 and 2:1 doped compounds were taken.

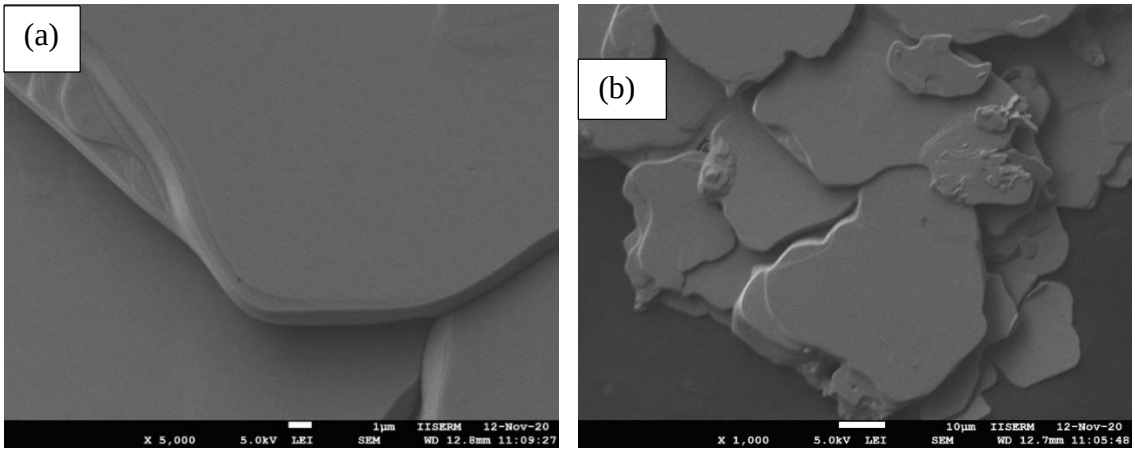

Figure 24. SEM images of undoped $(BA)_2PbCl_4$.

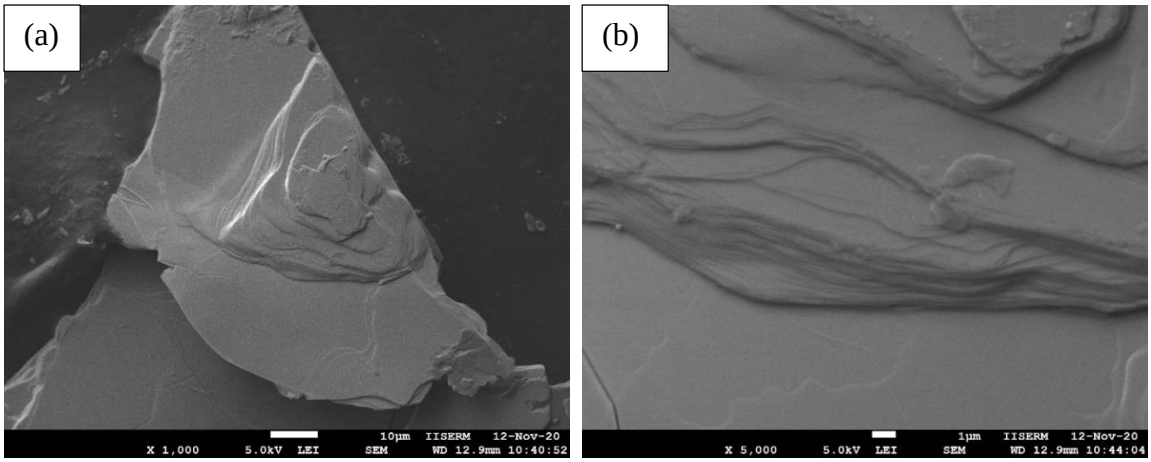

Figure 25. SEM images of 0.5:1 [Cu:Pb] doped $(BA)_2PbCl_4$.

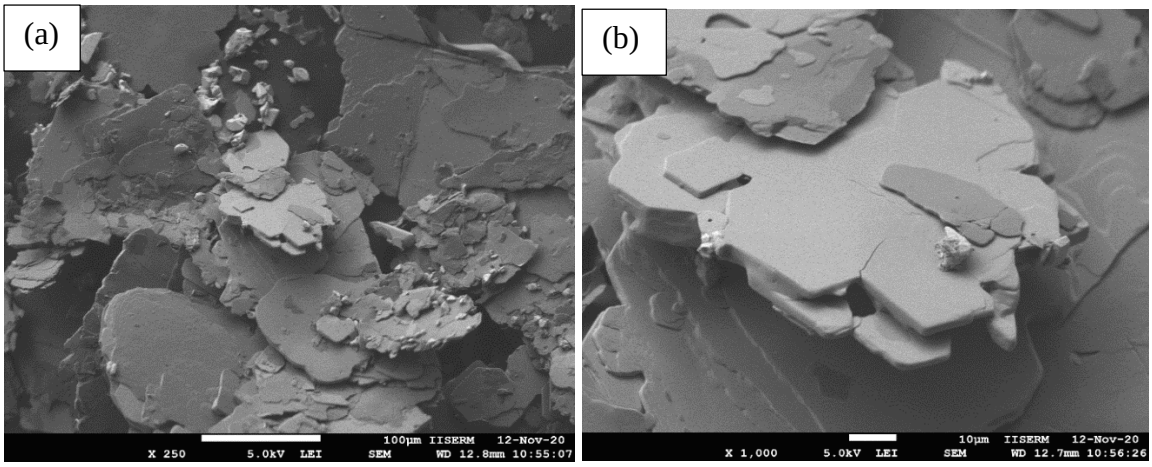

Figure 26. SEM images of 1:1 [Cu:Pb] doped $(BA)_2PbCl_4$.

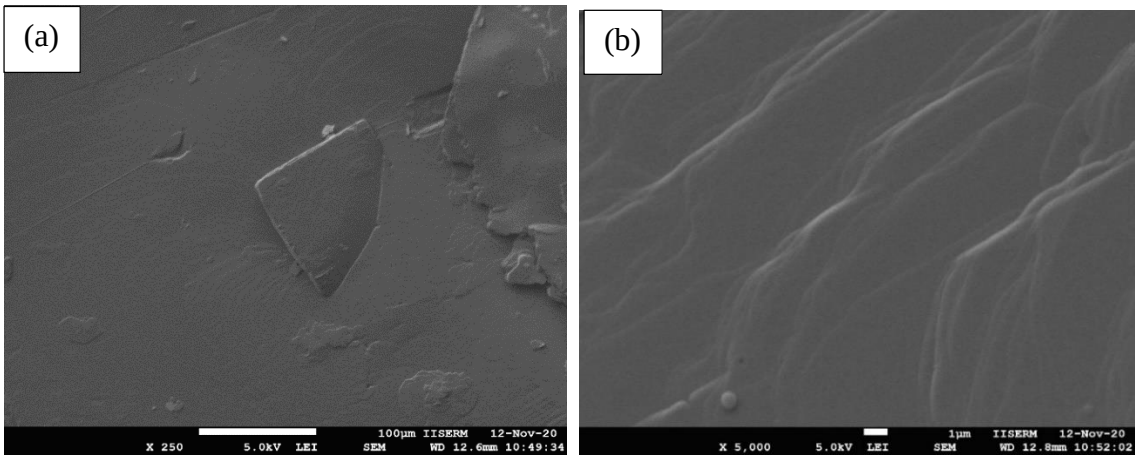

Figure 27. SEM images of 2:1 [Cu:Pb] doped $(BA)_2PbCl_4$.

The SEM images indicate formation of sheet like microstructures.

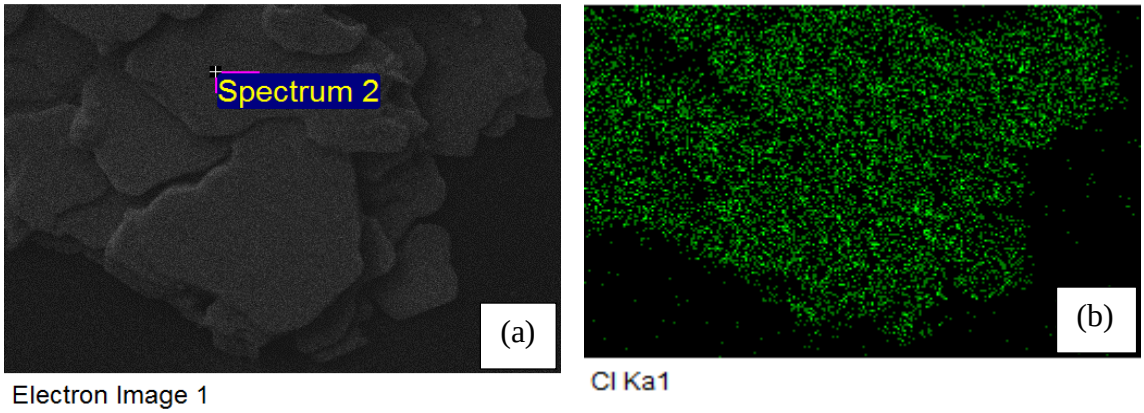

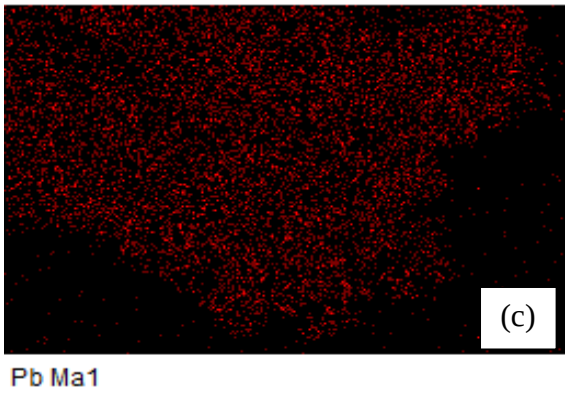

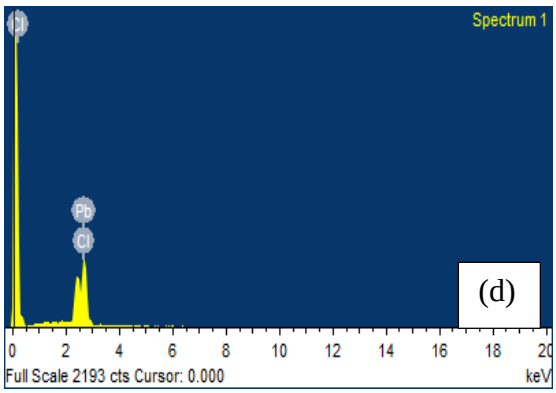

Element	Weight %	Atomic %
Cl K	46.38	83.49
Pb M	53.62	16.51

Figure 28. Elemental colour mapping (b, c, d) and EDS (e) data of undoped $(BA)_2PbCl_4$.

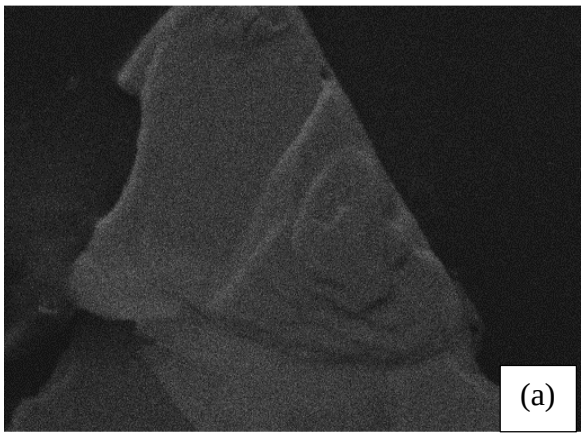

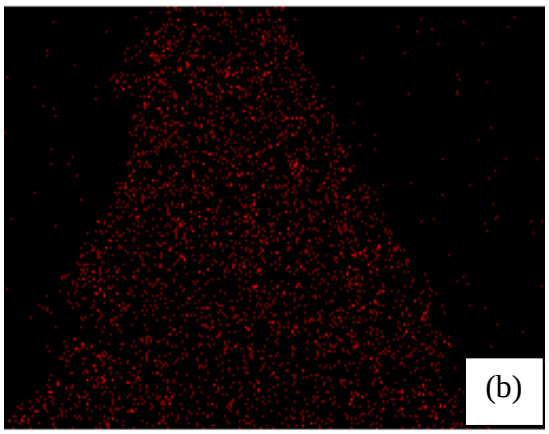

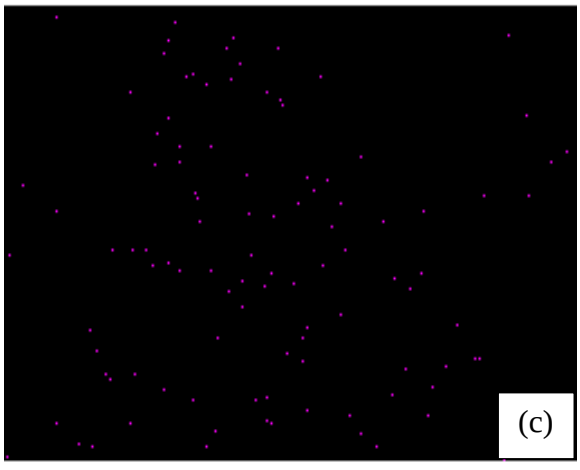

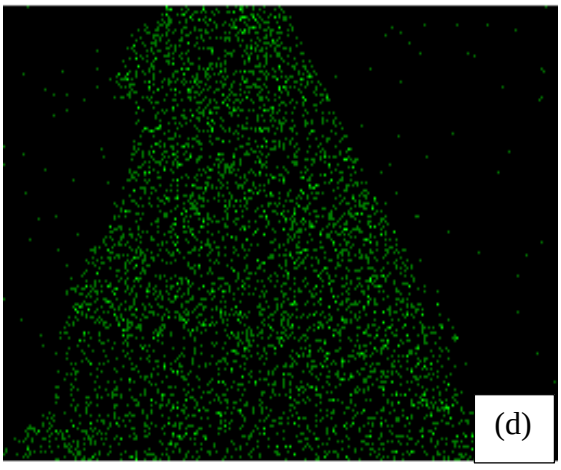

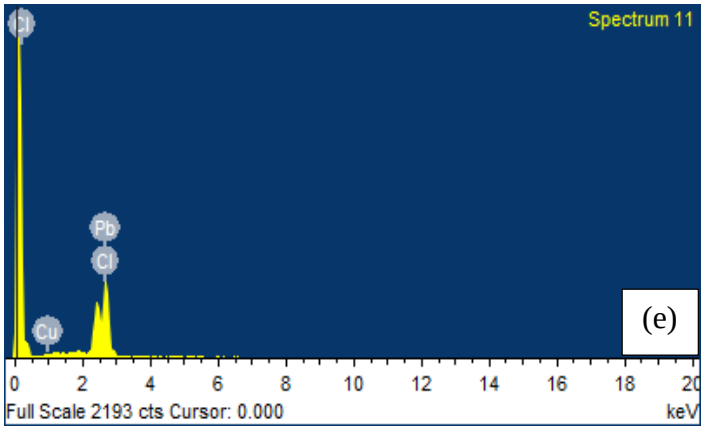

Element	Weight %	Atomic %
Cl K	46.80	83.35
Pb M	52.57	16.02
Cu	0.64	0.63

Figure 29. Elemental colour mapping (b, c, d) and EDS (e) data of 0.5:1 [Cu:Pb] $(BA)_2PbCl_4$.

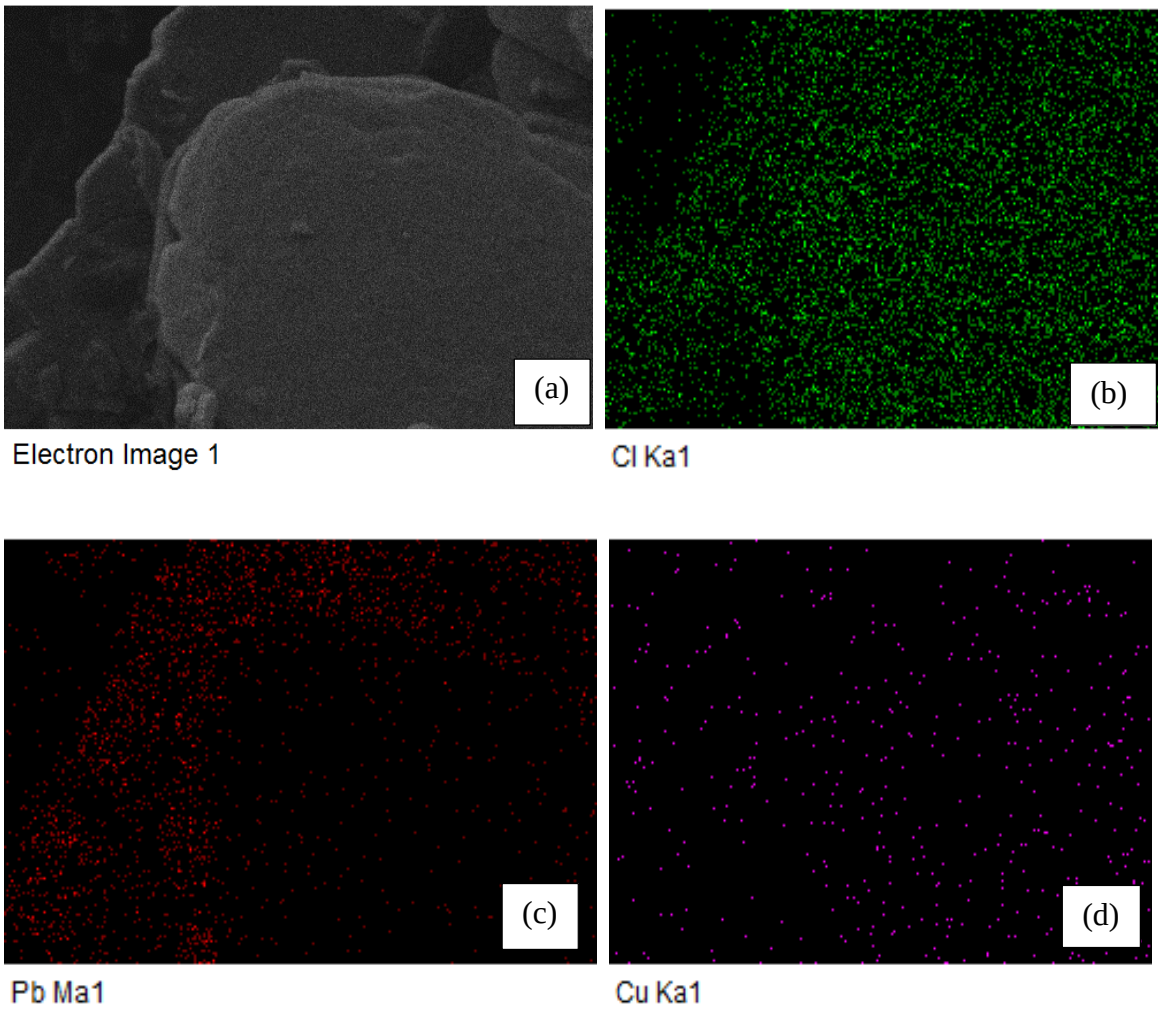

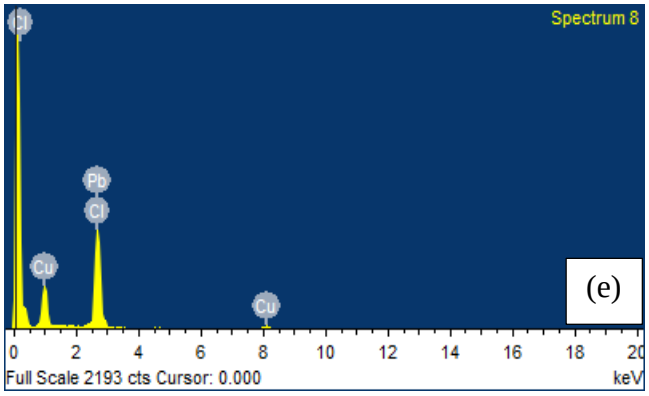

Element	Weight %	Atomic %
Cl K	61.54	74.89
Pb M	2.13	0.44
Cu	36.33	24.67

Figure 30. Elemental colour mapping (b, c, d) and EDS (e) data of 1:1 [Cu:Pb] $(BA)_2PbCl_4$.

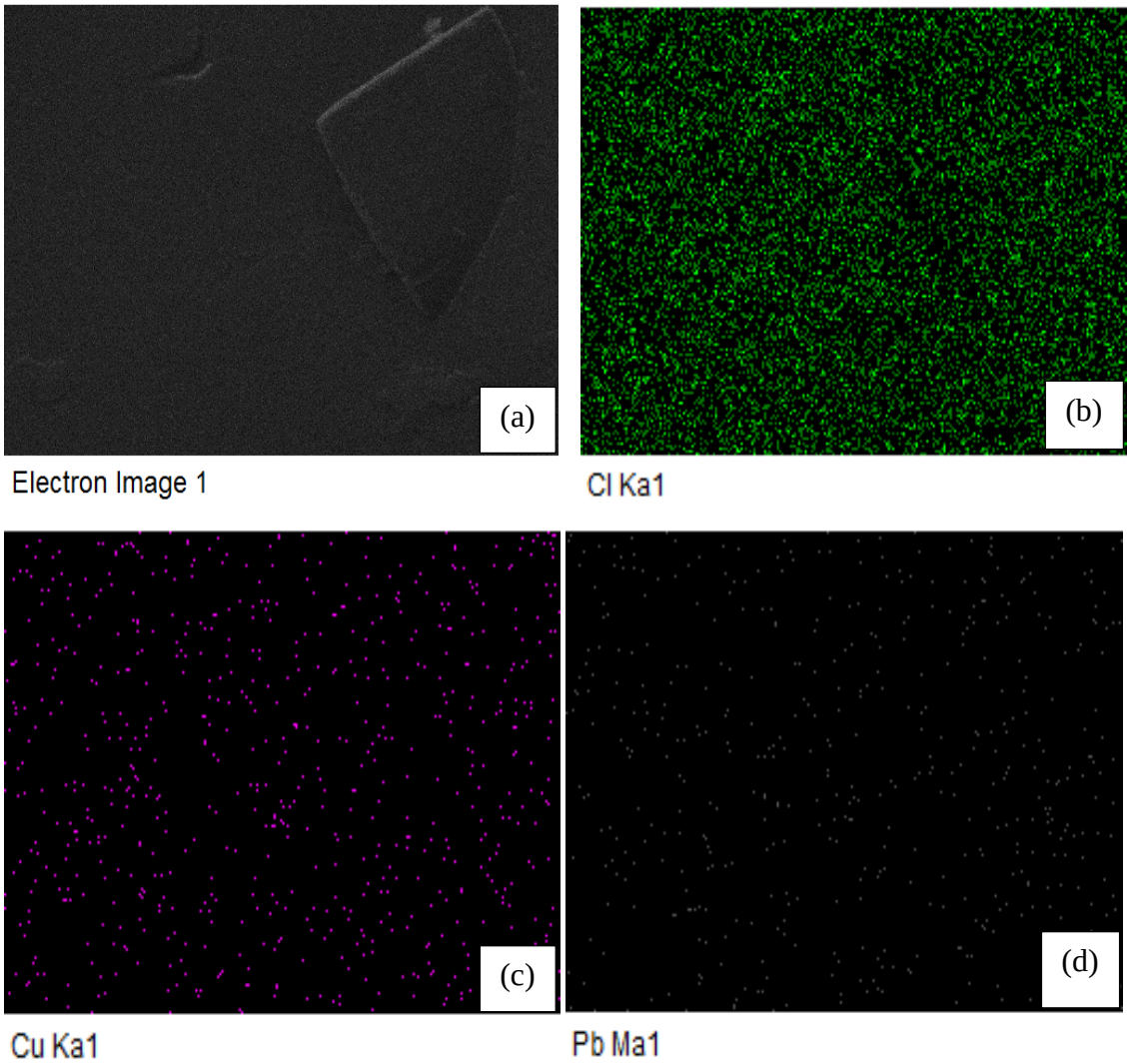

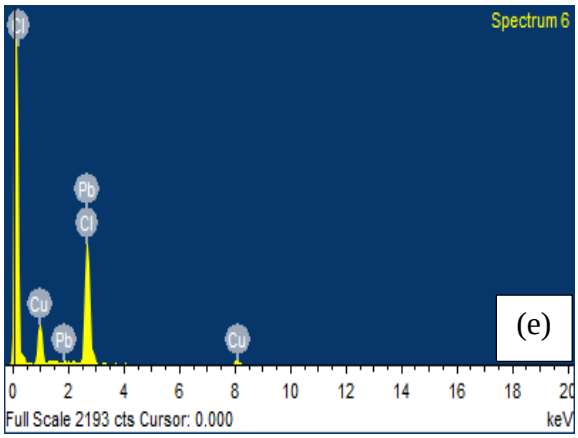

Element	Weight %	Atomic %
Cl K	55.80	70.90
Pb M	4.55	0.99
Cu	39.64	28.11

Figure 31. Elemental colour mapping (b, c, d) and EDS (e) data of 2:1 [Cu:Pb] $(BA)_2PbCl_4$.

The atomic percentage of Lead reduced to 0.44 % from 16.51 % on moving from undoped to 2:1 Cu:Pb, while the Copper content increased from 0.63 % to 24.67 %. This corroborates the assumption that increasing Cu content in the reaction mixture leads to replacement of Lead in the system.

To understand the lower limit to which Copper doping effectively happened, very low concentrations of Copper from 0.01 mmol to 0.04 mmol was added along with 1 mmol of Lead. The XRD data obtained is plotted here.

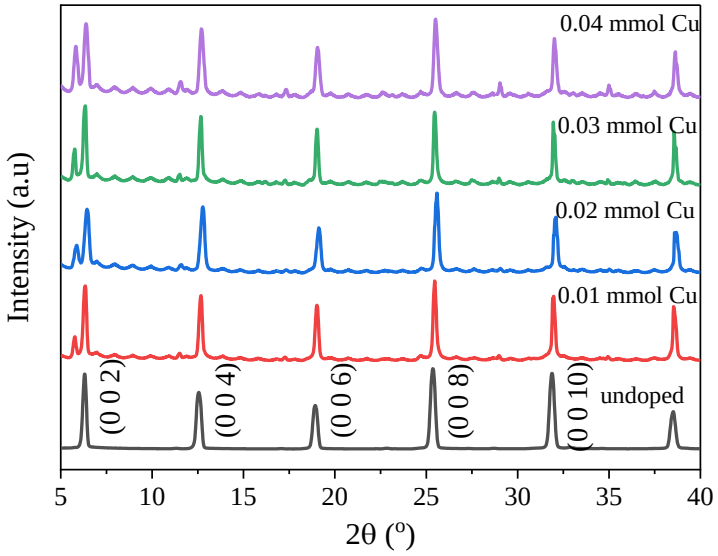

Figure 32. PXRD data of $(BA)_2PbCl_4$ doped with 0.01 mmol to 0.04 mmol of Cu.

New peaks corresponding to $(BA)_2CuCl_4$ starts appearing from 0.04 mmol of Copper. Entire planes corresponding to $CuCl_6$ octahedra starts forming from this dopant

concentration. Lower angle PXRD data was carefully analysed to understand the subtle difference in structure occurring due to doping.

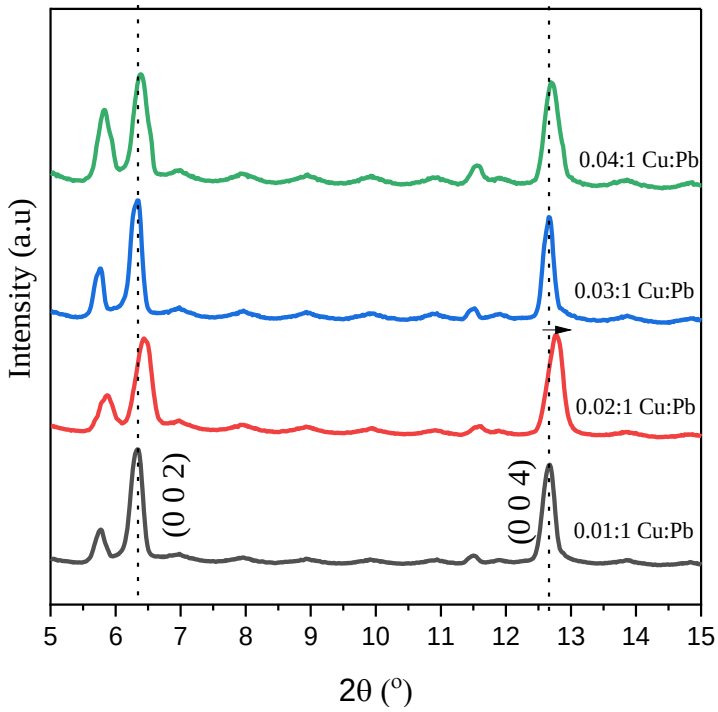

Figure 33. Low angle PXRD of $(BA)_2PbCl_4$ doped with 0.01 mmol to 0.04 mmol Cu.

Shifting of the PXRD peaks to higher angles was observed when 0.02 mmol Cu was doped with 1 mmol Pb. This correctly represents lattice contraction due to replacement of a larger atom Pb by the smaller atom Cu.[36]

It can be concluded from the PXRD analysis that at very low concentrations of Cu, lattice contraction occurs, but with increasing Cu content a heterogeneous system consisting of two phases forms, corresponding to the $CuCl_6$ and $PbCl_6$ octahedral planes followed by complete replacement of the $PbCl_6$ octahedra by the $CuCl_6$ octahedra at higher concentrations. A transition from pure $(BA)_2PbCl_4$ to pure $(BA)_2CuCl_4$ follows through a composite system containing both $PbCl_6$ and $CuCl_6$ octahedral planes.

To understand the effect of increasing dopant concentration on the interaction between the organic and inorganic components of the perovskites, Infrared studies were done.

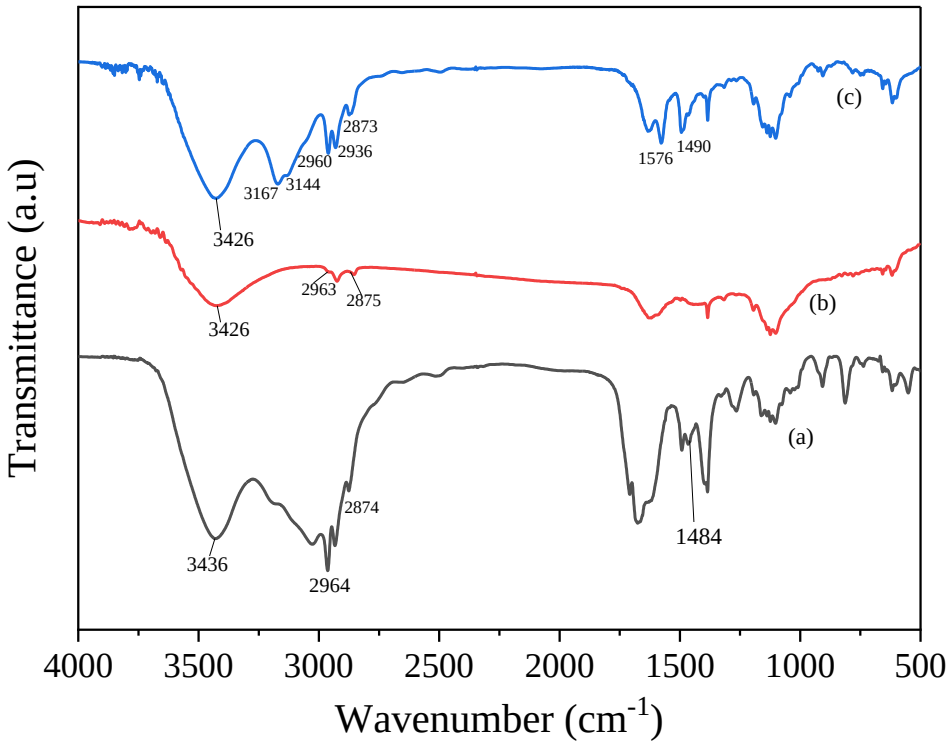

Figure 34. Infrared spectra of (a) $C_4H_9NH_3Cl$ (b) $(C_4H_9NH_3)_2PbCl_4$ (c) 4:1 [Cu:Pb] $(C_4H_9NH_3)_2PbCl_4$.

The stretching peaks of NH^{3+} shifts to higher wavenumbers (3167 and 3144 cm^{-1}) in (c) compared to $C_4H_9NH_3Cl$, but is lower than that of butylamine (3332 cm^{-1}). This is due to the self-assembling of NH^{3+} groups leading to a change in the chemical environment. Other peaks corresponding to asymmetric stretching (CH_3 – 2961 cm^{-1}, CH_2- 2933 cm^{-1}); symmetric stretching (CH_2- 2875 cm^{-1}); NH_2 bending (1576 cm^{-1}); is also present.[37]

2.2.4 STABILITY TESTS

To examine the effect of doping on the stability of the system, TGA of undoped $(BA)_2PbCl_4$ and Cu^{2+} doped $(BA)_2PbCl_4$ was done.

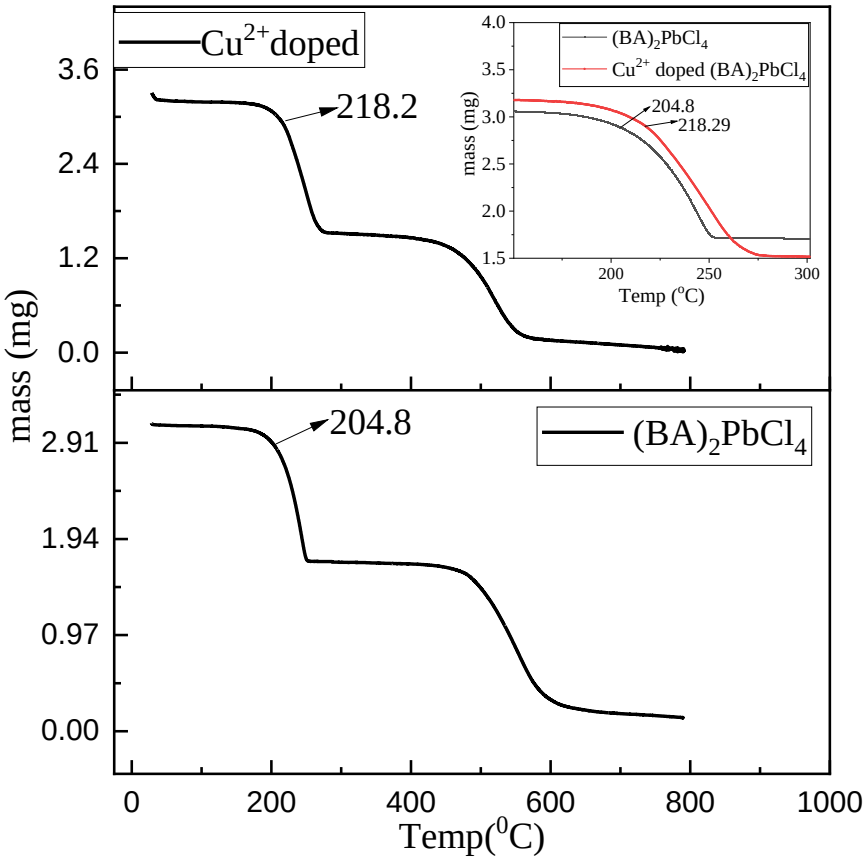

Figure 35. TGA data of Cu^{2+} doped $(BA)_2PbCl_4$ and $(BA)_2PbCl_4$.

The thermal decomposition temperature of the Cu^{2+} doped system was slightly higher than that of the pure $(BA)_2PbCl_4$, doping does not drastically change the degradation temperature of the sample. The initial weight loss is attributed to the two step dissociation of the organic component. Subsequent loss in weight might be due to the decomposition of metal halide.[38]

Thermal stability tests of $(BA)_2PbCl_4$ and 1:1 Cu:Pb doped $(BA)_2PbCl_4$ was done by heating both the samples at 110 ^oC for 6 days.

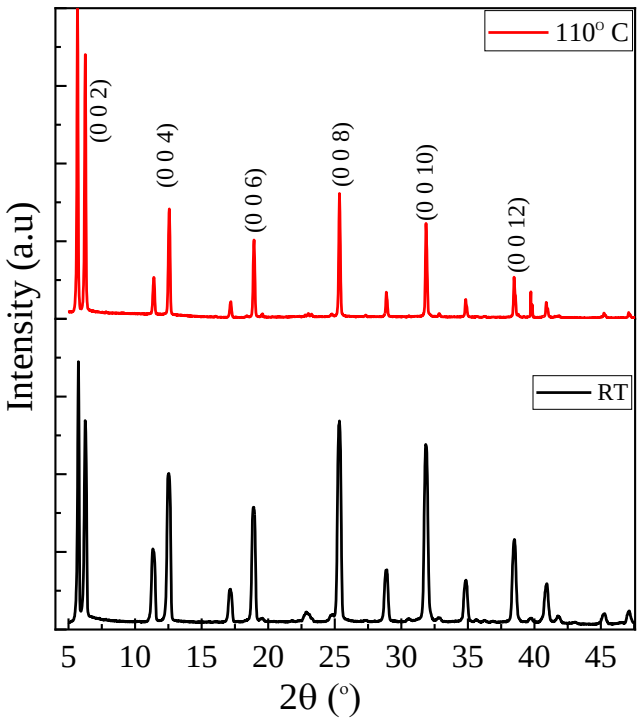

Figure 36. PXRD results for thermal stability test of 1:1 [Cu^{2+}: Pb] doped $(BA)_2PbCl_4$.

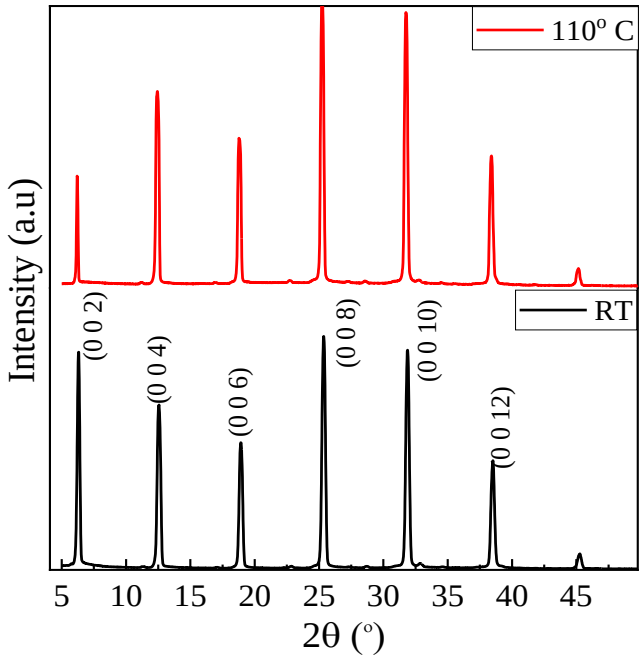

Figure 37. PXRD results for thermal stability test of undoped $(BA)_2PbCl_4$.

The XRD peaks of the samples heated at 110 °C did not show any noticeable change compared to those kept at ambient temperatures indicative of the fact that both the doped and the undoped samples were resistant to exposure to harsh temperatures.

Moisture stability tests of the undoped and doped system was conducted by heating in a humid chamber at 60 ^{o}C for 1 month.

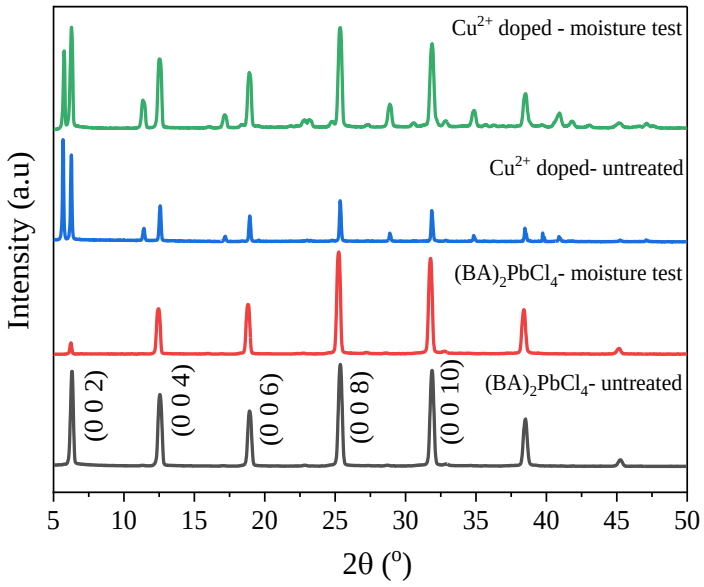

Figure 38. PXRD of the samples of moisture test.

The PXRD peaks of pure $(BA)_2PbCl_4$ and doped $(BA)_2PbCl_4$ did not show any noticeable changes. Both $(BA)_2PbCl_4$ and doped $(BA)_2PbCl_4$ are stable when heated in moisture.

2.3 CONCLUSION

Successful doping of Cu on $(C_4H_9NH_3)_2PbCl_4$ was done. White coloured crystals turned yellow on doping with a reduction of bandgap from 3.5 eV to 2.3 eV. Both CuCl and $CuCl_2$ had similar optical and structural effects on the compound, with Cu existing in +2 oxidation state in both the samples. The doped and pure $(BA)_2PbCl_4$ are found to be thermal and moisture stable. Their initial decomposition temperatures started above 200 ℃ indicating good thermal stability. Increasing the dopant concentration led to replacement of Lead Chloride octahedral with Copper Chloride octahedral resulting in the formation of $(C_4H_9NH_3)_2CuCl_4$.

2.4 FUTURE OUTLOOK

Further doping studies on the Bromine and Iodine analogues of $(BA)_2PbCl_4$ can also be done and its effect on the optical and structural properties can be studied. It is expected that the higher halide analogues will have a lower bandgap than $(BA)_2PbCl_4$. Doping can reduce the bandgap even further to enable their efficient usage in photovoltaic applications. Fabrication of single junction solar cells using these materials and its efficiency in solar devices can be explored.

Photocatalytic reactions can be done to compare the use of undoped and doped samples in activating various organic reactions. Kinetic studies on their influence on the rate of the reaction can be done and further experiments can be designed to elucidate the mechanism through which these photocatalysts influence reactions.

Bibliography

1. Kay, H. F.; Bailey, P. C. Structure and Properties of $CaTiO_3$. *Acta Cryst.* **1957**, *10*, 219-226.
2. Jin Y. K.; Jin W. L.; Hyun S. J.; Hyunjung S.; and Nam G. P. High-Efficiency Perovskite Solar Cells; *Chem. Rev.* **2020**, *120*, 7867-7918.
3. Rao, C.N.R. Encyclopedia of Physical Science and Technology (Third Edition), John Wiley & Sons, **2003**, pp 707-714.
4. Chouhan, L.; Ghimire, S.; Subrahmanyam, C.; Miyasaka, T.; Biju, V. Synthesis, optoelectronic properties and applications of halide perovskites. *Chem. Soc. Rev.*, **2020**, *49*, 2869-2885.
5. Shamsi, J.; Urban, S. A.; Imran, M.; Trizio, D. L.; Manna, L.; Metal Halide Perovskite Nanocrystals: Synthesis, Post-Synthesis Modifications, and Their Optical Properties. *Chem. Rev.* **2019**, *119*, 3296–3348.
6. Mao, L.; Stoumpos, C. C.; Kanatzidis, M. G.; Two-dimensional Hybrid Halide Perovskites: Principles and Promises, *J. Am. Chem. Soc.* **2019**, *141*, 1171–1190.
7. Aleksandrov, K. S. Structural Phase Transitions in Layered Perovskite like Crystals. *Crystallogr. Rep.* **1995**, *40*, 279-301.
8. Lan, C.; Zhou, Z.; Wei, R.; Ho, J. C.; Two-dimensional perovskite materials: From synthesis to energy-related applications. *Mater. Tod. Energy*, **2019**, *11*, 61-82.
9. Mao, L.; Ke, W.; Pedesseau, L.; Wu, Y.; Katan, C.; Even, J.; Wasielewski, M. R.; Stoumpos, C. C.; Kanatzidis, M. J., Hybrid Dion–Jacobson 2D Lead Iodide Perovskites. *J. Am. Chem. Soc.* **2018**, *140*, 3775–3783.
10. Soe, C. M. M.; Stoumpos, C. C.; Kepenekian, M.; Traoré, B.; Tsai, H.; Nie, W.; Wang, B.; Katan, C.; Seshadri, R.; Mohite, A. D.; Even, J.; Marks, T. J.; Kanatzidis, M. G. New Type of 2D Perovskites with Alternating Cations in the Interlayer Space, $(C(NH_2)_3)(CH_3NH_3)_nPb_nI_{3n+1}$: Structure, Properties, and Photovoltaic Performance. *J. Am. Chem. Soc.* **2017**, *139*, 16297-16309.
11. Stoumpos, C. C.; Cao, D. H.; Clark, D. J.; Young, J.; Rondinelli, J. M.; Jang, J. I.; Hupp, J. T.; Kanatzidis. M. G. Ruddlesden-Popper Hybrid Lead Iodide Perovskite 2D Homologous Semiconductors. *Chem. Mater.* **2016**, *28*, 2852−2867.

12. Li, X.; Hoffman, J. M.; Kanatzidis, M. G. The 2D Halide Perovskite Rulebook: How the Spacer Influences Everything from the Structure to Optoelectronic Device Efficiency. *Chem. Rev.* **2021,** *121,* 2230-2291.

13. Luo, B.; Guo, Y.; Li, X.; Xiao, Y.; Huang, X.; Zhang, J. Z. Efficient Trap-Mediated Mn^{2+} Dopant Emission in Two Dimensional Single-Layered Perovskite $(CH_3CH_2NH_3)_2PbBr_4$. *J. Phys. Chem. C* **2019**, *123,* 14239−14245.

14. Li, X.; Hoffman, J.; Ke, W.; Chen, M.; Tsai, H.; Nie, W.; Mohite, A. D.; Kepenekian, M.; Katan, C.; Even, J.; et al. Two Dimensional Halide Perovskites Incorporating Straight Chain Symmetric Diammonium Ions, $(NH_3C_mH_{2m}NH_3)$-$(CH_3NH_3)_{n-1}Pb_nI_{3n+1}$ (m = 4−9; n = 1−4). *J. Am. Chem. Soc.* **2018**, *140,* 12226−12238.

15. Cervantes, C. O.; Monroy, P. C.; Ibarra, D. S.; Two-Dimensional Halide Perovskites in Solar Cells: 2D or not 2D? *ChemSusChem.* **2019**, *12,* 1560-1575.

16. Guo Z.; Wu X.; Zhu T.; Zhu, X.; Huang, L. Electron–Phonon Scattering in Atomically Thin 2D Perovskites. *ACS Nano* **2016**, *10*, 9992-9998.

17. Cortecchia, D.; Mróz, W.; Neutzner, S.; Borzda, T.; Folpini, G.; Petrozza, A. M. Mn(II)-doped 2D perovskite for light emitting devices. Italiano, I. No Title. No. Ii, 24–30.

18. Gao, X.; Zhang, X.; Yin, W.; Wang, H.; Hu, Y.; Zhang, Q.; Shi, Z.; Colvin, V. L.; Yu, W. W.; Zhang, Y. Ruddlesden–Popper Perovskites: Synthesis and Optical Properties for Optoelectronic Applications. *Adv. Sci.* **2019**, *6,* 1900941-1900963.

19. Koutselas, I. B.; Ducasse, L.; Papavassiliou, G. C. Electronic properties of three- and low-dimensional semiconducting materials with Pb halide and Sn halide units. *J. Phy.: Condens. Matter.* **1996**, *8,* 1217-1227.

20. N. Kitazawa, Mater. Excitons in two-dimensional layered perovskite compounds: $(C_6H_5C_2H_4NH_3)_2Pb(Br,I)_4$ and $(C_6H_5C_2H_4NH_3)_2Pb(Cl,Br)_4$. *Sci. Eng. B* **1997,** *49,* 233-238.

21. Ma, L.; Ju, M. G.; Dai,J.; Zeng, X. C. Tin and germanium based two-dimensional Ruddlesden–Popper hybrid perovskites for potential lead-free photovoltaic and photoelectronic applications. *Nanoscale* **2018**, *10,* 11314-11319.

22. Fu, W.; Liu, H.; Shi, X.; Zuo, L.; Li, X.; Jen, A. K.-Y. Tailoring the Functionality of Organic Spacer Cations for Efficient and Stable Quasi-2D Perovskite Solar Cells. *Adv. Funct. Mater.* **2019**, *29,* 1900221 - 1900229.

23. Passarelli, J. V.; Fairfield, D. J.; Sather, N. A.; Hendricks, M. P.; Sai, H.; Stern,C. L.; Stupp, S. I.; Enhanced Out-of-Plane Conductivity and Photovoltaic Performance in *n* = 1 Layered Perovskites through Organic Cation Design. *J. Am. Chem. Soc.* **2018**, *140,* 7313-7323.

24. Zhang, X.; Ren, X.; Liu,B.; Munir, R.; Zhu, X.; Yang, D.; Li, J.; Liu, Y.; Smilgies, D-M.; Li, R; Yang, Z.; Niu, T.; Wang, W.; Amassian, A.; Zhao,K.; Liu,S.; Stable high efficiency two-dimensional perovskite solar cells *via* cesium doping. *Energy Environ. Sci.* **2017,** *10,* 2095-2102.

25. Biswas, A.; Bakthavatsalam,R.; Kundu,J.; Efficient Exciton to Dopant Energy Transfer in Mn^{2+} Doped $(C_4H_9NH_3)_2PbBr_4$ Two-Dimensional (2D) Layered Perovskites. *Chem. Mater.* **2017**, *29,* 7816−7825.

26. Dutta, S. K.; Dutta, A.; Adhikari, S. D.; Pradhan N. Doping Mn^{2+} in Single Crystalline Layered Perovskite Microcrystals. *ACS Energy Lett.* **2019**, *4*, 343−351.

27. Weidman, M. C.; Seitz, M.; Stranks, S. D.; Tisdale, W. A. Highly Tunable Colloidal Perovskite Nanoplatelets through Variable Cation, Metal, and Halide Composition. *ACS Nano* **2016**, *10,* 7830–7839.

28. Liao, Q.; Chen, J.; Zhou, L.; Wei,T; Zhang, L.; Chen, D.; Huang F.; Pang, Q.; Zhang, J. Z. Bandgap Engineering of Lead-Free Double Perovskite $Cs_2AgInCl_6$. Nanocrystals via Cu^{2+} Doping. *J. Phys. Chem. Lett.* **2020**, *11,* 8392−8398.

29. Karmakar, A.; Dodd, M. S.; Agnihotri, S.; Ravera, E.; Michaelis, V. K. Cu (II)-Doped $Cs_2SbAgCl_6$ Double Perovskite: A Lead-Free, Low-Bandgap Material. *Chem. Mater.* **2018**, *30,* 8280−8290.

30. Makuła, P.; Pacia, M.; Macyk, W. How to Correctly Determine the Band Gap Energy of Modified Semiconductor Photocatalysts Based on UV–Vis Spectra. *J. Phys. Chem. Lett.* **2018**, *9*, 6814–6817.

31. Zhou, G.; Guo, S.; Zhao, J.; Molokeev, M.; Liu, Q.; Zhang, J.; Xia, Z. Unraveling the mechanochemical synthesis and luminescence in Mn II-based two-dimensional hybrid perovskite $(C_4H_9NH_3)_2PbCl_4$. *Sci China Mater.* **2019**, *62,* 1013–1022.

32. Paul, T.; Maiti, S.; Besra, N.; Chatterjee, B. K.; Das, B. K.; Thakur, S.; Sarkar, S.; Das, N. S.; Chattopadhyay, K. K. Tailored $CsPbX_3$ Nanorods for Electron-Emission Nanodevices. *ACS Appl. Nano Mater.* **2019**, *2*, 5942–5951.

33. *Brundle, C. R.; Crist, B. V.;* X-ray photoelectron spectroscopy: A perspective on quantitation accuracy for composition analysis of homogeneous materials. *J. Vac. Sci. Technol. A* **2020,** *38,* 1-18.

34. Singhal, N.; Chakraborty, R.; Ghosh, P.; Nag, A. Low-Bandgap $Cs_4CuSb_2Cl_{12}$ Layered Double Perovskite: Synthesis, Reversible Thermal Changes, and Magnetic Interaction. *Chem. Asian J.* **2018**, *13*, 2085– 2092.

35. Liu, H.; Wang, X.; Hu, W.; Guo, L; Ouyang, S. Preparation and characterization of $(C_4H_9NH_3)_2CuX_4$ (X-Cl, Br). *Chem. J. Internet* **2004**, *6*, 066039ne.

36. Bi, C.; Wang, S.; Li, Q.; Kershaw, S. V.; Tian, J.; Rogach, A. L.; Thermally Stable Copper (II) Doped Cesium Lead Halide Perovskite Quantum Dots with a Strong Blue Emission. *J. Phys. Chem. Lett.* **2019**, *10*, 943–952.

37. Xiao, Z. L.; Chen, H. Z.; Shi, M. M.; Wu, G.; Zhou, R. J.; Yang, Z. S.; Wang, M.; Tang, B. Z. Preparation and characterization of organic–inorganic hybrid perovskite $(C_4H_9NH_3)_2CuCl_4$. *Mat. Sci. Eng. B Solid-State Mater. Adv. Technol.* **2005,** *117***,** 313–316.

38. Mitzi, D. B.; Prikas, M. T.; Chondroudis, K. Thin Film Deposition of Organic−Inorganic Hybrid Materials Using a Single Source Thermal Ablation Technique. *Chem. Mater.* **1999**, *11*, 542–544.